Energy level statistics of the two-dimensional Hubbard model at low filling

Henrik Bruus* and Jean-Christian Anglès d'Auriac†
Centre de Recherches sur les Très basses Températures, CNRS, Boîte Postale 166, F-38042 Grenoble Cédex 9, France
(Received 18 October 1996)

The energy level statistics of the Hubbard model for $L\times L$ square lattices ($L=3,4,5,6$) at low filling (four electrons) is studied numerically for a wide range of coupling strength. All known symmetries of the model (space, spin, and pseudospin symmetry) have been taken into account explicitly from the beginning of the calculation by projecting into symmetry-invariant subspaces. The details of this group theoretical treatment are presented with special attention to the nongeneric case of $L=4$, where a particular complicated space group appears. For all the lattices studied, a significant amount of levels within each symmetry invariant subspaces remains degenerated, but except for $L=4$ the ground state is nondegenerate. We explain the remaining degeneracies, which occur only for very specific interaction-independent states, and we disregard these states in the statistical spectral analysis. The intricate structure of the Hubbard spectra necessitates a careful unfolding procedure, which is thoroughly discussed. Finally, we present our results for the level spacing distribution, the number variance Σ^2, and the spectral rigidity Δ_3, which essentially all are close to the corresponding statistics for random matrices of the Gaussian ensemble independent of the lattice size and the coupling strength. Even very small coupling strengths approaching the integrable zero coupling limit lead to Gaussian ensemble statistics, stressing the nonperturbative nature of the Hubbard model. [S0163-1829(97)02613-1]

I. INTRODUCTION

The behavior of strongly correlated electronic systems remains a central problem in contemporary condensed matter physics. Several years of intense studies have made it clear that the necessary theoretical skills and tools to deal with strongly correlated fermion systems are lacking (see, e.g., the recent reviews by Dagatto[1] and Lieb[2]). Many exotic schemes have been invented to accommodate a suitable theoretical framework, but the development of a predictive general theory does not seem to be in sight. In this state of affairs the importance of performing numerical calculations of the ground-state properties and the energy spectrum of a given many-body Hamiltonian has grown. Computational results can lead to the acceptance or rejection of the proposed analytical models, and they can guide the development of new analytical approaches.

In the Hubbard model and related models one important parameter is the filling ν. Much work has been devoted to the high-density case near half filling, since it is believed to be relevant for high-temperature superconductivity,[1,3] but also the low-filling regime is of interest; e.g., it plays an important role in theoretical studies of the breakdown of Fermi liquid theory in two dimensions (2D).[4] In this paper we present a numerical study of the two-dimensional Hubbard model at the low-filling regime $\nu<0.25$, a regime where the calculation is tractable. It is natural to choose four particles as a generic case close to the simple two-particle case. The coupling strength is used as a perturbation parameter, and we address the question of universality in the response of strongly correlated electron systems to this perturbation.[5]

We describe an efficient method which allows for numerical calculations of the exact energy spectrum. This method can relatively easily be extended to calculations of various Green's functions and spectral functions well suited for the study of low-lying excitations and the corresponding coherent part of the spectral densities, a topic we will study in forthcoming work. Here, we rather study the statistical properties of the typical high-energy excitations which are related to the incoherent background of the typical spectral functions. More specifically, we study the statistical properties of the spectra within the framework of random matrix theory (RMT). RMT was developed for the study of neutron scattering resonances in nuclear physics in the 1950s and 1960s,[6] but it has since been applied to a wide range of problems in many areas of physics[7] (e.g., studies of conduction fluctuations,[8] microwave eigenmodes,[9] and acoustical properties of solids[10]) and mathematics (e.g., studies of the distribution of the zeros of the Riemann ζ function[11]). Moreover, RMT has also been applied to various types of matrix ensembles like Hamiltonian matrices[6] (as in our case) and scattering matrices,[8,12] as well as transfer matrices[13] and Glauber matrices[14] of statistical mechanics models. Recently, RMT has been employed in the study of strongly correlated electronic systems. Examples are studies of the 2D t-J model,[15] 2D tight-binding models,[16] the 1D Bethe chain,[17] and the 1D Luttinger liquid.[18] The work presented here with emphasis on mathematical and numerical methods is an extension of this line of research. Preliminary results of our work have been published elsewhere.[19]

There are basically two ways of applying RMT. One way is to model a relevant matrix of the given physical system with a matrix drawn from a suitable random matrix ensemble and subsequently calculate average properties of the system by averaging over the random matrix ensemble according to RMT. The other way, which we employ here, consists simply of characterizing the spectrum of a given physical system by comparing various statistical properties of the spectrum with the corresponding properties calculated within one of the few universal statistical matrix ensembles of RMT. Which of these ensembles describes properly a physical situ-

ation depends on the symmetries of the system. The given spectrum which one analyzes is of course deterministic, but statistical properties are given to it by considering quantities like, for example, the distribution of the energy spacings where all but one of the spectral variables have been integrated out. This is like pseudo-random-number generators which are perfectly deterministic and nevertheless have many properties in common with random sequences.

The paper is organized as follows. In Sec. II we introduce the Hubbard model and the corresponding Hilbert space. In Sec. III we introduce the RMT quantities used in the characterization of the spectra, and we discuss in detail the special spectral unfolding technique necessitated by the intricate nature of the Hubbard spectra. In Sec. IV the entire symmetry group consisting of space, spin, and pseudospin symmetry of the model is studied, and all the corresponding projection operators are calculated. In Sec. V the model is diagonalized numerically and we study the raw spectrum, in particular the ground state and some unexpected remaining degeneracies higher in the spectrum. In Sec. VI we present the result of the spectral statistics analysis of the model, and finally, in Sec. VII we discuss the results and conclude. Appendixes A–D contain mathematical details.

II. HUBBARD MODEL

Throughout this paper we study the simple one-band $L\times L$ square lattice Hubbard model with periodic boundary conditions containing a nearest-neighbor hopping term $-t\hat{T}$ and an on-site interaction term $U\hat{U}$:

$$\hat{H}=-t\hat{T}+U\hat{U}=-t\sum_{\langle i,j\rangle,\sigma}^{L^2}\hat{c}_{j\sigma}^{\dagger}\hat{c}_{i\sigma}+U\sum_{i}^{L^2}\hat{n}_{i\uparrow}\hat{n}_{i\downarrow}, \quad (1)$$

where $\hat{c}_{i\sigma}^{\dagger}$ and $\hat{n}_{i\sigma}$ are the creation operator and the number operator, respectively, for an electron on site i with spin σ. No disorder is present in the model. Below half filling the dimension N_H of the Hilbert space grows rapidly as a function of L and the number N_e of electrons occupying the lattice, and so we have confined ourselves to the low-filling case of only four electrons, whereas we let L vary. Moreover, without loss of generality we always work in the sector where the z component S_z of the total spin is zero; the other S_z sectors can be reached by use of the spin ladder operators S_+ and S_-, which commute with the Hamiltonian. The $S_z=0$ sector is the largest of the spin sectors, and it has $N_H=[L^2(L^2-1)/2]^2$ which for $L=3$, 4, 5, and 6, the lattice sizes studied here, yields 1296, 14 400, 90 000, and 396 900, respectively. The corresponding fillings $\nu\equiv N_e/2L^2$ are 0.22, 0.13, 0.08, and 0.06.

In the occupation number basis we label the states as follows,[20] where a and b are two lattice sites occupied with spin-up electrons and c and d with spin-down electrons:

$$|a,b;c,d\rangle\equiv\hat{c}_{a\uparrow}^{\dagger}\hat{c}_{b\uparrow}^{\dagger}\hat{c}_{c\downarrow}^{\dagger}\hat{c}_{d\downarrow}^{\dagger}|\mathrm{vac}\rangle. \quad (2)$$

Two explicit examples of such states as well as the lattice site enumeration are shown in Fig. 1. In our work we make sure that $a<b$ and $c<d$, and we have ordered the basis states such that the state $|x_1,x_2;x_3,x_4\rangle$ comes before the state $|x_1',x_2';x_3',x_4'\rangle$ if $x_i<x_i'$, where i is the first position

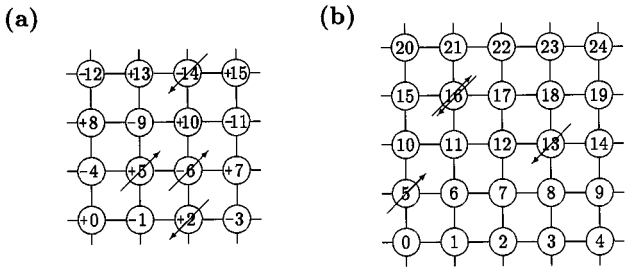

FIG. 1. Two four-electron states with $S_z=0$ are shown: in (a) the zero-pair state $|5,6;2,14\rangle$ of the 4×4 square lattice and in (b) the one-pair state $|5,16;13,16\rangle$ of the 5×5 square lattice. The convention of the ket notation is explained in the text. The numbering of the lattice sites is the one employed in our computer calculations. The signs of the 4×4 lattice correspond to the bipartition of the lattice, which is only possible for even site lattices.

encountered where x_i and x_i' are different. If during a calculation a state is encountered with $a>b$ and/or $c>d$, the necessary exchange operations including sign changes are performed to restore it.

Finally we note that for even L a bipartition of the lattice is possible. A given lattice site a can be identified by a set of Cartesian coordinates $\mathbf{a}=(a_1,a_2)$ simply counting the position in the lattice [thus, e.g., site $0=(0,0)$ and $9=(1,2)$ in Fig. 1(a)]. Each site a can then be assigned with a sign $\theta_a\equiv(-1)^{a_1+a_2}=\exp(i\boldsymbol{\pi}\cdot\mathbf{a})$, where $\boldsymbol{\pi}=(\pi,\pi)$.

III. RANDOM MATRIX THEORY

Within random matrix theory (RMT) one can study several statistical ensembles of matrices. Three important examples are the diagonal ensembles, the Gaussian ensembles for Hermitian matrices as, e.g., Hamiltonians, and the circular ensembles for unitary matrices as, e.g., scattering matrices. Since a main object of this work is to characterize the spectrum of the Hubbard model within the framework of RMT, we are led to use the diagonal and the Gaussian ensembles of square matrices. The first ensemble is the ensemble of diagonal matrices D with statistically independent diagonal elements D_{ii} drawn from the same distribution $P(D_{ii})$. This ensemble describes situations where the eigenvalues are essentially independent, which empirically has been found to be the case for integrable models. One characteristic feature of such systems is a ''soft'' spectrum with large probabilities of having levels close together described by the Poisson (exponential) distribution. The three others ensembles—denoted the Gaussian orthogonal ensemble (GOE), Gaussian unitary ensemble (GUE), and Gaussian symplectic ensemble (GSE)—are defined by requirering statistical independence of the matrix elements of a matrix H and invariance of the probability distribution $P(H)$ in matrix space under one of the three canonical similarity transformations: the orthogonal, the unitary, and the symplectic transformations, respectively.[6] Which ensemble to choose depends on the symmetry of the system. In fact, the ensembles are universal in the sense that no details of the physical system play any role; only knowledge of the global symmetry is needed. The three Gaussian ensembles are found to describe situations of very complex or chaotic systems, and one char-

acteristic feature of such systems is a ''rigid'' spectrum with eigenvalue repulsion. In this work we need only to treat the GOE, which is found for systems with preserved time-reversal symmetry.

To perform a meaningful RMT analysis one has to sort the spectrum in symmetry sectors corresponding to the symmetry group of the Hamiltonian since the symmetry-invariant subspaces are orthogonal to one another. Each such symmetry-invariant subspace is characterized by a specific set of quantum numbers, and the RMT analysis is performed on sets of eigenlevels having the same quantum numbers. In Sec. IV we treat the complete symmetry group of the Hubbard model and calculate the corresponding projection operators of the symmetry-invariant subspaces. As illustrated in Sec. VI significant errors are introduced in the analysis if some of the symmetries are neglected.

Another caveat in the RMT analysis of finite spectra is the notion of mixed phase space. As a function of some external parameter a given system can be driven from integrability (the diagonal ensemble) to chaos (one of the Gaussian ensembles) or from one type of symmetry (say, the GOE) to another (say, the GUE). If the spectrum of such a system is studied in the middle of the transition, the spectrum is a mixture of two or more components, each described by one of the random ensembles.[21] In the thermodynamic limit usually only one component survives, but for finite spectra this mixing calls for a further sorting of the spectrum within each symmetry-invariant subspace. For the Hubbard model using the coupling strength U/t as the external parameter such a situation does in fact arise as the analysis presented in Sec. VB shows.

When the necessary sorting of the spectrum has been performed the RMT analysis can begin. The first step is to unfold the spectrum.

A. Unfolding the spectrum

Naturally, it is necessary to make some kind of transformation or normalization of the spectrum of any given physical system to be able to make comparisons with the universal and dimensionless results of RMT. This operation is called the unfolding. By local rescaling of the spectrum with the local average level spacing the unfolding transforms the actual energies E_i into dimensionless ''unfolded energies'' ε_i with a local density of 1. Thus, by unfolding one subtracts the regular slowly varying part of the spectrum and considers only the fluctuations. It amounts to computing from the actual integrated density of states $N(E)$,

$$N(E)=\int_{-\infty}^{E}\sum_i \delta(e-E_i)\,de=\sum_i \theta(e-E_i), \qquad (3)$$

an averaged integrated density of state $\overline{N}(E)$. The unfolded energies ε_i are then given by

$$\varepsilon_i=\overline{N}(E_i). \qquad (4)$$

The notions of ''local density'' and ''averaged density'' are not mathematically rigorous. For some systems there exists natural unfolding procedures. For example, it is a rigorous result that the density of states for a $N\times N$ random matrix approaches a semicircular form for $N\to\infty$; thus for any given finite random matrix one simply uses the limiting density of states as the average density. In billiard systems one can make a Laurent series expansion in $\sqrt{E}$ of $N(E)$ and obtain the Weyl law for $\overline{N}(E)$ by truncating the series after a finite number of terms, each of which has a physical interpretation. In our case, no such natural choices exist for $\overline{N}(E)$. We have therefore used several methods to unfold the spectra. Each of these methods has a free parameter, but there is no unique prescription of how to choose it. The best criterion is the insensitivity of the final result to the method employed and to reasonable variations of the free parameter.

The first method is polynomial interpolation. It can be a simple linear interpolation or running average where $\overline{N}(E_i)$ is found as a linear fit of $N(E)$ in an interval containing r levels on each side of the level E_i; the free parameter is then the parameter r. It can also be higher order polynomial interpolation, e.g., in the form of interpolating between several linear interpolations—a method we used in our work on statistical mechanics models.[13,22]

The second method[7] defines $\varepsilon_i=\varepsilon_{i-1}+d_1/d_n$, where d_k is the kth smallest spacing to E_i. Here n becomes the free parameter. This method works also for complex eigenvalues of non-Hermitian matrices.

The third method is Fourier broadening of the step functions $\theta(e-E_i)$ in Eq. (3). The Fourier transforms from the energy domain to the time domain of the step functions are found. In the following back transformation yielding $\overline{N}(E)$ only the slow time components are kept. Choosing a cutoff τ beyond which all Fourier components are set to zero yields $\theta(e-E_i)\approx \mathrm{Si}[(e+E^*-E_i)\tau]/\pi-\mathrm{Si}[(e-E^*+E_i)\tau]/\pi$, where $\mathrm{Si}(x)$ is the sine integral and E^* is an energy slightly larger than the largest energy in the spectrum to be unfolded. The free parameter is τ, and by choosing $1/\tau$ to be of the order of the mean-level spacing a good $\overline{N}(E)$ is obtained.

The fourth method is Gaussian broadening of the delta functions $\delta(e-E_i)$ in Eq. (3), leading to the following expression for $\overline{N}(E)$:

$$\overline{N}(E)=\int_{-\infty}^{E}\sum_i \frac{1}{\sigma_i\sqrt{2\pi}}\exp\left[-\frac{(e-E_i)^2}{2\sigma_i^2}\right]de. \qquad (5)$$

The standard deviation or width σ_i of the Gaussians can be taken as a constant for the entire spectrum; it is then the free parameter. However, due to the appearance of many minibands in the Hubbard spectrum for small values of U/t each having different densities, it is desirable to let σ_i adapt to local variations in the spectrum. We have developed the following algorithm: Take α levels to each side of level i, determine the local average level spacing $\Delta_i=(E_{i+\alpha}-E_{i-\alpha})/(2\alpha)$, and set $\sigma_i=0.608\alpha\Delta_i$. By this assignment 90% of the weight of the broadened peak falls in the interval $[E_i-\alpha\Delta_i,E_i+\alpha\Delta_i]$ and α becomes the free parameter. If a gap (defined as a very atypical spacing) falls within the chosen range, we only take the states of the same side of the gap as E_i into account. The procedure is illustrated in Fig. 2. We discuss how to optimize the choice of α in Sec. VI. Typically, we find $\alpha\approx 4$ to be a good choice.

All four methods of unfolding yield essentially the same results. We decided to use the Gaussian broadening with varying width, Eq. (5), since it was better suited to the study

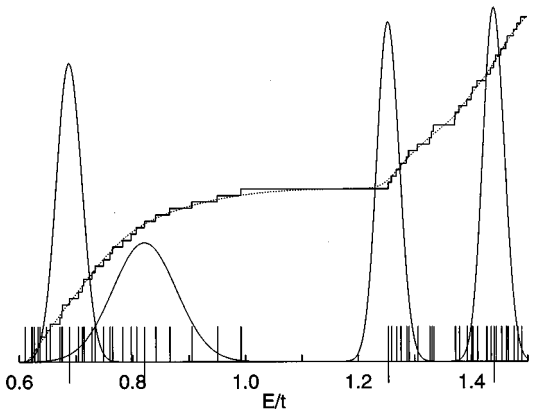

FIG. 2. Unfolding of the spectrum using the Gauss broadening with variable width, choosing $\alpha=4$. Shown is a part of the Hubbard spectrum of the invariant subspace $(R,S)=(6,0)$ around $E/t\approx 1.1$ for $L=5$ and $U/t=1$. The positions of the levels E_i are marked by short vertical lines. For four levels marked by long vertical lines we show the actual broadened Gaussians. Note how the widths of the Gaussians change as the local density of states changes, and note how the width of the Gaussian centered near the gap ignores the states beyond the gap. Also shown are the level staircase $N(E)$ and the averaged integrated density of states $\overline{N}(E)$ (the smooth dotted line).

of the Hubbard spectra with its many minibands at small coupling strength U/t (see Sec. V A).

A final remark on the unfolded spectrum is that it is customary to discard from the analysis the states closest to the boundary of the spectrum or to the edges of the minibands. The reason is that these levels in contrast to the levels in the bulk of the spectrum do not interact with levels of both higher and lower energy. Hence such levels are nongeneric. We usually discarded a few percent of the total number of states on that account. This effect is a size effect that is expected to be negligible in the thermodynamic limit.

B. Quantities characterizing the spectrum

The simplest quantity one studies in RMT analysis is the probability distribution $P(s)$ of unfolded energy spacings $s=\varepsilon_i-\varepsilon_{i-1}$, where ε_i and ε_{i-1} are two consecutive unfolded energies. One compares the actual $P(s)$ with the same quantity obtained for random matrices from one of the matrix ensembles introduced in Sec. III. For diagonal random matrices $P(s)$ is the Poisson (exponential) distribution $P(s)=\exp(-s)$. For $N\times N$ GOE matrices the distribution of spacings is quite complicated for arbitrary N; however, it is always close to the exact spacing distribution of the 2×2 GOE matrices known as the Wigner surmise,

$$P^{\mathrm{GOE}}(s)=\frac{\pi}{2}s\exp\left(-\frac{\pi}{4}s^2\right), \tag{6}$$

which therefore is used in practice.

The spacing distribution probes correlations between consecutive states and is not sensitive to correlations of higher order. For example, an artificial spectrum constructed by adding independent variables distributed according to Eq. (6) will certainly show a Wignerian spacing distribution but has clearly nothing else in common with GOE spectra. To test higher-order correlations one then looks at the two-point correlation function $Y(x)$ and various weighted averages thereof.[6] For the GOE in the large-N limit,

$$Y(x)=s(x)^2+\frac{ds(x)}{dx}\int_x^\infty s(t)\,dt,$$

with $s(x)=\sin(\pi x)/(\pi x)$. One average of $Y(x)$ often studied is the number variance $\Sigma^2(\lambda)$ defined as the variance of the number of unfolded energy levels in intervals of length λ around the unfolded energy ε_0:

$$\Sigma^2(\lambda)=\left\langle\left[N_u\left(\varepsilon_0+\frac{\lambda}{2}\right)-N_u\left(\varepsilon_0-\frac{\lambda}{2}\right)-\lambda\right]^2\right\rangle_{\varepsilon_0}, \tag{7}$$

where $N_u(\varepsilon)\equiv\Sigma_i\theta(\varepsilon-\varepsilon_i)$ is the unfolded level staircase, and where the brackets denote an averaging over ε_0. For the Poissonian case $\Sigma^2(\lambda)=\lambda$, while for the GOE case $\Sigma^2(\lambda)=\lambda-2\int_0^\lambda(\lambda-x)Y(x)\,dx$ with a logarithmic asymptotic behavior.

Another average of the two-point correlation function is the spectral rigidity $\Delta_3(\lambda)$ defined as the least-squares deviation of the unfolded level staircase $N_u(\varepsilon)$ from the best-fitting straight line in an interval of length λ:

$$\Delta_3(\lambda)=\left\langle\frac{1}{\lambda}\min_{(A,B)}\int_{\varepsilon_0-\lambda/2}^{\varepsilon_0+\lambda/2}[N_u(\varepsilon)-A\varepsilon-B]^2d\varepsilon\right\rangle_{\varepsilon_0}. \tag{8}$$

For the Poissonian case the spectral rigidity is $\Delta_3(\lambda)=\lambda/15$, while for the GOE case $\Delta_3(\lambda)=[\lambda-\int_0^\lambda f(x)Y(x)\,dx]/15$, with $f(x)=(\lambda-x)^3(2\lambda^2-9\lambda x-3x^2)/\lambda^4$ and again with a logarithmic asymptotic behavior.

IV. GROUP THEORY AND INVARIANT SUBSPACES

The problem of diagonalizing the Hubbard Hamiltonian can be reduced considerably by group theoretical analysis. Furthermore, as mentioned earlier and as illustrated by an example in Sec. VI A it is indispensable for the RMT analysis. The symmetries are explicitly dealt with from the beginning of the calculation by constructing the symmetry projection operators corresponding to all known symmetries of the model and using them to project into symmetry-invariant subspaces of the full Hilbert space.[23,24] The main object of this section is to construct the three projection operators $\mathcal{P}_R$, $\mathcal{P}_S$, and $\mathcal{P}_J$ corresponding to the space symmetry, the spin symmetry, and the pseudospin symmetry, respectively.

A. Space symmetry group

The first symmetry we consider is the space group G_L of the $L\times L$ square lattice with periodic boundary conditions. It consists of all permutations g of the sites such that $g(i)$ and $g(j)$ are neighbors if and only if i and j are neighbors. In a straightforward manner an operator $\hat{g}$ in Hilbert space can be associated with each element g of G_L, $\hat{g}|a,b;c,d\rangle\equiv|g(a),g(b);g(c),g(d)\rangle$, thus forming a group $\hat{G}_L$ of operators, which commutes with the Hubbard Hamiltonian $\hat{H}$. For general values of L the space group G_L has been ana-

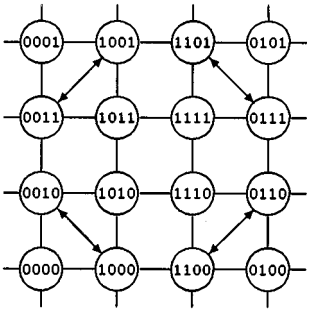

FIG. 3. The mapping of the 4×4 square lattice with periodic boundary conditions onto the unit hypercube in 4D. The four double arrows indicate the neighbor-preserving transformation r_h. This transformation cannot be expressed by the ordinary translations and reflections in 2D; however, it can be interpreted as a hyperplane reflection in 4D around the xz plane.

lyzed in detail in Ref. 20. Here we will restrict ourselves to outlining this analysis and to correcting the particular cases of $L=2$, which induces a simpler space group, and $L=4$, which induces a much richer space group as briefly mentioned in Ref. 25.

For $L\neq2,4$ the structure of G_L can simply be built up by forming direct[26] and semi-direct[27] products, denoted $\otimes$ and $\circledS$, respectively, of translation and reflection subgroups. Let T_x (T_y) be the subgroups of order L of translations (isomorphic with $\mathcal{Z}_L$) in the x (y) direction, and let r_x, r_y, and r_d be the reflection operations for the x axis, the y axis, and the diagonal defined by $r_x(x)=-x$, $r_y(y)=-y$, and $r_d(x,y)=(y,x)$, while e denotes the identity transformation. The two subgroups $G_L^x=T_x\circledS\{e,r_x\}$ and $G_L^y=T_y\circledS\{e,r_y\}$ of order $2L$ (isomorphic with $C_{Lv}=\mathcal{Z}_L\circledS\mathcal{Z}_2$) are formed and combined into the direct product subgroup $G_L^{xy}=G_L^x\otimes G_L^y$. Finally G_L is formed by the semidirect product $G_L=G_L^{xy}\circledS\{e,r_d\}$. One can say that G_L is generated by the elements $\{t_x,r_x,t_y,r_y,r_d\}$ although this is not the smallest possible set of generators. The order N_L of $G_L=(C_{Lv}\otimes C_{Lv})\circledS\mathcal{Z}_2$ is seen to be $N_L=8L^2$.

For $L=2$ we find $G_2=(\{e,r_x\}\otimes\{e,r_y\})\circledS\{e,r_d\}=C_{4v}$ with $N_2=8$. This result differs from that of the general case since $t_x=r_x$ and $t_y=r_y$.

For the case $L=4$ a richer group appears because the 4×4 lattice with periodic boundary conditions is isomorphic with the group of transformations of the four-dimensional unit hypercube. This isomorphism is easily seen by changing the decimal enumeration of Fig. 1(a) into a binary enumeration such that the binary numbers of neighboring sites differ by only 1 bit as shown in Fig. 3. They can immediately be interpreted as the coordinates of the corners of the hypercube. Thus the group G_4 of neighbor-preserving transformations is given by combining bit inversion operations $0\leftrightarrow1$ with permutations of the 4 bits. In Appendix A we show that G_4 is isomorphic with the group $(\mathcal{Z}_2\otimes\mathcal{Z}_2\otimes\mathcal{Z}_2\otimes\mathcal{Z}_2)\circledS S_4$ corresponding to the semidirect product of all combinations of bit inversions at the four positions with the permutation group S_4 of the four positions. One neighbor-preserving transformation of the lattice which is not given by products of the elements $\{t_x,r_x,t_y,r_y,r_d\}$ is the hyperplane reflection r_h (see Fig. 3) obtained in 4D by a reflection in the xz plane while keeping y and w fixed. G_4 can be generated by replacing r_d above with r_h (we note that $r_d=t_x^{-1}t_y^{-1}r_ht_yt_xr_h$), and a set of generators is $\{t_x,r_x,t_y,r_y,r_h\}$ though in fact as few as two elements can be found that generate G_4.[28] Instead of 128 elements found by the formula $N_L=8L^2$, we find $N_4=2^4\times4!=384$. We refer the reader to Appendix A and Appendix B for further details concerning G_4 and G_L, respectively.

The complete table of characters $\chi_R^{(R')}(g)$ of G_4 is given in Table IV in Appendix A, while those of G_3, G_5, and G_6 are found by combining Table V in Appendix B with the method of Ref. 20. Armed with the character tables the character projection operator $\hat{\mathcal{P}}_R^{(R')}$ (where the subscript R is used to distinguish from S and J) can be constructed for each $l_{R'}$-dimensional irreducible representation R':

$$\hat{\mathcal{P}}_R^{(R')}\equiv\frac{l_{R'}}{N_L}\sum_{g\in G_L}\chi_R^{(R')*}(g)\hat{g}. \tag{9}$$

Using $\hat{\mathcal{P}}_R^{(R')}$ for a given representation together with the Van Vleck basis-function generating algorithm[23,24] in the actual or a closely related Hilbert space it is straightforward to construct an orthonormal l_R-dimensional basis $\{\phi_1^{(R)},\phi_2^{(R)},\ldots,\phi_{l_R}^{(R)}\}$ and calculate an explicit irreducible representation matrix $\Gamma_{ij}^{(R)}(g)\equiv\langle\phi_i^{(R)}|\hat{g}|\phi_j^{(R)}\rangle$. Finally the row projection operator $\hat{\mathcal{P}}_{Rk}^{(R')}(g)$ can be constructed:

$$\hat{\mathcal{P}}_{Rk}^{(R')}\equiv\frac{l_{R'}}{N_L}\sum_{g\in G_L}\Gamma_{kk}^{(R')*}(g)\hat{g}. \tag{10}$$

Both projection operators $\hat{\mathcal{P}}_R^{(R')}$ and $\hat{\mathcal{P}}_{Rk}^{(R')}$ will be employed in the diagonalization of the Hubbard Hamiltonian.

B. SU(2) spin symmetry

It is easily verified that the Hubbard Hamiltonian, Eq. (1), commutes with the z component of the total spin operator $\hat{S}_z=\Sigma_{i=1}^{N_e}\hat{S}_z^{(i)}$ as well as with the corresponding raising and lowering operators $\hat{S}_+$ and $\hat{S}_-$. The model therefore possesses a SU(2) spin symmetry. We can therefore restrict our diagonalization to the $S_z=0$ sector, since the other sectors can be reached using the spin-raising and -lowering operators. The spin operators also commute with any space symmetry operator $\hat{g}$, and so the two symmetry groups form a direct product group. The combination of two spin-up and two spin-down electrons under the constraint $S_z=0$ leads to a total spin quantum number $S'=0$, 1, or 2. The explicit construction in Appendix C with $\hat{O}=\hat{\mathbf{S}}^2$ yields the following three spin projection operators $\hat{\mathcal{P}}_S^{(S')}$:

$$\begin{aligned}\hat{\mathcal{P}}_S^{(0)}|a,b;c,d\rangle=\tfrac{1}{6}(&+2|a,b;c,d\rangle+|a,c;b,d\rangle-|a,d;b,c\rangle\\&+2|c,d;a,b\rangle+|b,d;a,c\rangle-|b,c;a,d\rangle),\end{aligned} \tag{11}$$

$$\hat{\mathcal{P}}_S^{(1)}|a,b;c,d\rangle=\tfrac{1}{6}(+3|a,b;c,d\rangle-3|c,d;a,b\rangle), \tag{12}$$

$$\hat{\mathcal{P}}_S^{(2)}|a,b;c,d\rangle = \tfrac{1}{6}(+1|a,b;c,d\rangle - |a,c;b,d\rangle + |a,d;b,c\rangle + 1|c,d;a,b\rangle - |b,d;a,c\rangle + |b,c;a,d\rangle). \tag{13}$$

These expressions are generally valid; however, one should note that the Pauli exclusion principle reduces the number of terms when electron pairs are present. For example, if $a=c$ and $b=d$, one finds $\mathcal{P}_S^{(S')}|a,b;c,d\rangle = \delta_{S',0}|a,b;c,d\rangle$. Finally we note that the spin projectors of the state $|a,b;c,d\rangle$ involve all six states generated by permutations of the site indices. In Eqs. (11)–(13) only three orthogonal states appear. The remaining three orthogonal states are the two $S=1$ states $|a,c;b,d\rangle - |b,d;a,c\rangle$ and $|a,d;b,c\rangle - |b,c;a,d\rangle$ and the one $S=0$ state $|a,c;b,d\rangle + |b,d;a,c\rangle + |a,d;b,c\rangle + |b,c;a,d\rangle$.

C. SU(2) pseudospin symmetry

The pseudospin symmetry of the Hubbard model has been known for at least a quarter of century,[29] but recently it was rediscovered and put in the more generalized context of the η-pairing mechanism.[30,31] As discussed in Sec. II even L lattices can be biparted using the site sign θ_i as an index, and three operators $\hat{J}_-$, $\hat{J}_+$, and $\hat{J}_z$ can be defined:

$$\hat{J}_- = \sum_i \theta_i \hat{c}_{i\uparrow}\hat{c}_{i\downarrow}, \quad \hat{J}_+ = \sum_i \theta_i \hat{c}^\dagger_{i\downarrow}\hat{c}^\dagger_{i\uparrow}, \quad \hat{J}_z = \frac{1}{2}\sum_{i\sigma} \hat{n}_{i\sigma} - \frac{L^2}{2}. \tag{14}$$

It is seen that $\hat{J}_+$ creates a pair of electrons with phase θ_i on empty sites i. These three operators form the same algebra as $\hat{S}_-$, $\hat{S}_+$, and $\hat{S}_z$, hence the name pseudospin. Furthermore, the $\hat{J}$ operators commute with both the space symmetry operators and the spin operators; and for the symmetrized Hubbard model $\hat{H}'$,[32] trivially related to our model $\hat{H}$, they even commute with the Hamiltonian $\hat{H}'$. Hence the (symmetrized) model possesses an extra SU(2) symmetry characterized by the quantum numbers J' and J_z analogous to S' and S_z for the spin.[33] A detailed analysis shows that the combination of spin and pseudospin symmetries yields $[\mathrm{SU}(2)\otimes\mathrm{SU}(2)]/\mathcal{Z}_2 = \mathrm{SO}(4)$ rather than the full $\mathrm{SU}(2)\otimes\mathrm{SU}(2)$.[31] The space symmetry group is completely independent of spin and pseudospin symmetries. Thus the full symmetry group for L even is $\mathcal{G} = G_L \otimes \mathrm{SO}(4)$ while for L odd it is $\mathcal{G} = G_L \otimes \mathrm{SU}(2)$. In our case the symmetry is lowered in a trivial way from spherical to cylindrical symmetry in pseudospin space since $[\hat{U}, \hat{J}_\pm] = \pm\hat{J}_\pm$, but still we have $[\hat{H}, \hat{J}^2] = [\hat{H}, \hat{J}_z] = 0$ and J' and J_z both remain good quantum numbers.

For a given lattice with even L containing a fixed number N_e of electrons all states have $J_z = (N_e - L^2)/2$ (e.g., -6 for $L=4$ and -16 for $L=6$). Defining $J_0 \equiv |J_z|$, the size J of the pseudospin in this situation takes the values $J_0, J_0+1, \ldots, J_0+N_e/2$. The projection operators $\hat{\mathcal{P}}_J^{(J')}$ are found using the construction of Appendix C with $\hat{O} = \hat{J}^2 = \hat{J}_+\hat{J}_- + \hat{J}_z^2 - \hat{J}_z$. Due to the explicit reference to pairs in the definition of the pseudospin operators, it has proved useful to introduce a special notation for one-pair and two-pair basis states as follows:

$$|P;b,d\rangle \equiv \theta_P c^\dagger_{P\downarrow} c^\dagger_{P\uparrow} c^\dagger_{b\uparrow} c^\dagger_{d\downarrow}|\mathrm{vac}\rangle = \theta_P |P,b;P,d\rangle,$$
$$|P;Q\rangle \equiv \theta_P\theta_Q c^\dagger_{P\downarrow} c^\dagger_{P\uparrow} c^\dagger_{Q\downarrow} c^\dagger_{Q\uparrow}|\mathrm{vac}\rangle = -\theta_P\theta_Q |P,Q;P,Q\rangle. \tag{15}$$

For zero-pair states where a, b, c, and d are all different, only $\hat{\mathcal{P}}_J^{(J'=J_0)}$ is nonzero,

$$\hat{\mathcal{P}}_J^{(J_0)}|a,b;c,d\rangle = |a,b;c,d\rangle, \tag{16}$$

and for one-pair states where P, b, and d are all different, two projection operators are nonzero,

$$\hat{\mathcal{P}}_J^{(J_0)}|P;b,d\rangle = \frac{2J_0+1}{2(J_0+1)}|P;b,d\rangle + \frac{-1}{2(J_0+1)}\sum_{Q\neq P,b,d}|Q;b,d\rangle, \tag{17}$$

$$\hat{\mathcal{P}}_J^{(J_0+1)}|P;b,d\rangle = \frac{1}{2(J_0+1)}|P;b,d\rangle + \frac{1}{2(J_0+1)}\sum_{Q\neq P,b,d}|Q;b,d\rangle, \tag{18}$$

while for two-pair states where $P\neq Q$, all three projection operators are nonzero:

$$\hat{\mathcal{P}}_J^{(J_0)}|P;Q\rangle = \frac{\Sigma_{R\neq P,Q}\Sigma_{S\neq P,Q,R}|R;S\rangle}{2(J_0+1)(2J_0+3)} + \frac{(2J_0+1)|P;Q\rangle}{2J_0+3} - \frac{(2J_0+1)\Sigma_{R\neq P,Q}\{|R;Q\rangle + |R;P\rangle\}}{2(J_0+1)(2J_0+3)}, \tag{19}$$

$$\hat{\mathcal{P}}_J^{(J_0+1)}|P;Q\rangle = \frac{-\Sigma_{R\neq P,Q}\Sigma_{S\neq P,Q,R}|R;S\rangle}{2(J_0+1)(J_0+2)} + \frac{|P;Q\rangle}{J_0+2} + \frac{J_0\Sigma_{R\neq P,Q}\{|R;Q\rangle + |R;P\rangle\}}{2(J_0+1)(J_0+2)}, \tag{20}$$

$$\hat{\mathcal{P}}_J^{(J_0+2)}|P;Q\rangle = \frac{\Sigma_{R\neq P,Q}\Sigma_{S\neq P,Q,R}|R;S\rangle}{2(J_0+2)(2J_0+3)} + \frac{|P;Q\rangle}{(J_0+2)(2J_0+3)} + \frac{\Sigma_{R\neq P,Q}\{|R;Q\rangle + |R;P\rangle\}}{(J_0+2)(2J_0+3)}. \tag{21}$$

At this stage all the group theoretical ingredients are ready for the diagonalization of the Hubbard Hamiltonian.

D. Symmetry-invariant subspaces

Using the projection operators the N_H-dimensional Hilbert space can be broken down into smaller symmetry invariant subspaces. Let $\mathcal{G}$ be the group containing the symmetry operations γ, each being a product of a space symmetry transformation, a spin rotation, and (for L even) a pseudospin rotation, $\gamma = g\otimes g_S \otimes g_J$. Here $\mathcal{G}$ thus consists of one finite group and one or two compact Lie groups. Let ρ be a multi-index describing an irreducible representation $\Gamma^{(\rho)}$ of $\mathcal{G}$. For

TABLE I. For $L=3$, 4, 5, and 6 are shown the dimension N_H of the total unreduced Hilbert space and the dimension $\max\{a_\rho\}$ of the largest symmetry-invariant subspace. Since matrix diagonalization is an n^3 operation, the number $\Sigma_\rho a_\rho^3/N_H^3$ provides an estimate of the relative reduction in computer time by projecting into the invariant subspaces.

	$L=3$	$L=4$	$L=5$	$L=6$
N_H	1296	14 400	90 000	396 900
$\max_\rho\{a_\rho\}$	38	146	1794	5490
$\Sigma_\rho a_\rho^3/N_H^3$	14.1×10^{-5}	0.7×10^{-5}	2.3×10^{-5}	1.0×10^{-5}

even [odd] L we have $\rho=(R',S',J')$ $[\rho=(R',S')]$. The ''celebrated'' theorem[23,24] states how many times a_ρ each row of the irreducible representation $\Gamma^{(\rho)}$ with character $\chi^{(\rho)}$ appears in any given not necessarily irreducible representation Γ with character χ:

$$a_\rho=\frac{1}{N_L}\sum_{G_L}\int_{\mathrm{SU}(2)}dg_S\int_{\mathrm{SU}(2)}dg_J\chi^{(\rho)*}(\gamma)\chi(\gamma). \quad (22)$$

We now choose Γ to be the following N_H-dimensional reducible representation:

$$\Gamma_{ij}(\gamma)\equiv\langle i|\hat{\gamma}|j\rangle, \quad \chi(\gamma)=\sum_{i=1}^{N_H}\langle i|\hat{\gamma}|i\rangle. \quad (23)$$

Inserting into Eq. (22) these $\chi(\gamma)$'s which are directly linked to Hilbert space yield

$$a_\rho=\int_{\mathcal{G}}d\gamma\chi^{(\rho)*}(\gamma)\sum_{i=1}^{N_H}\langle i|\hat{\gamma}|i\rangle=\frac{1}{l_R}\sum_{i=1}^{N_H}\langle i|\hat{\mathcal{P}}^{(\rho)}|i\rangle$$
$$=\frac{1}{l_R}\sum_{i=1}^{N_H}\langle i|\hat{\mathcal{P}}_R^{(R')}\otimes\hat{\mathcal{P}}_S^{(S')}\otimes\hat{\mathcal{P}}_J^{(J')}|i\rangle, \quad (24)$$

which is obtained by using $\chi(\gamma)=\chi(g\otimes g_S\otimes g_J)=\chi(g)\chi(g_S)\chi(g_J)$ and the definitions of the character projection operators. Note that only the space group projection needs a normalizing factor $1/l_R$. The spin and pseudospin are both restricted to take only one value of their respective z component; hence their normalizing factor is 1.

The initial size of the Hubbard Hamiltonian to be diagonalized is $[L(L-1)/2]^2$. However, only states transforming according to the same row of the same irreducible representation ρ can have a nonzero matrix element. Hence the Hamiltonian matrix breaks up in blocks, one per representation, and within each representation a further division into l_R equivalent blocks occurs. The relationship between N_H, $a_{(R',S',J')}$, and $l_{R'}$ is $N_H=\Sigma_{(R,S,J)}l_{R'}a_{(R',S',J')}$. This reduction is considerable as shown in Table I.

V. NUMERICAL DIAGONALIZATION OF THE HUBBARD MODEL

The numerical calculation of the exact spectra of the Hubbard model begins by determining the block size a_ρ for all the irreducible representations ρ. Then for a given $\rho=(R',S',J')$, where J' is disregarded in case of odd L, an a_ρ-dimensional orthonormal basis is found by using the projection operator

$$\hat{\mathcal{P}}_0^{(\rho)}\equiv\hat{\mathcal{P}}_{R0}^{(R')}\otimes\hat{\mathcal{P}}_S^{(S')}\otimes\hat{\mathcal{P}}_J^{(J')}, \quad (25)$$

which projects onto the first row of the space group representation R' with the spin index S' and pseudospin index J'. The projection operator $\hat{\mathcal{P}}_0^{(\rho)}$ is applied on one basis state after another while performing an ongoing Gram-Schmidt orthonormalization procedure. This yields new basis states $|w_i\rangle$, and when a_ρ such states are found, the procedure is terminated.

The next step is to calculate the kinetic energy and potential energy matrix elements $\langle w_i|\hat{T}|w_j\rangle$ and $\langle w_i|\hat{U}|w_j\rangle$. These matrix elements are stored in the computer and thereafter it is a simple matter to pick any value of U/t and diagonalize the Hubbard Hamiltonian, $\hat{H}=-t\hat{T}+U\hat{U}$, using standard diagonalization routines. The calculation of the symmetry invariant matrix blocks of $\hat{T}$ and $\hat{U}$ takes the amount of time of the order of one diagonalization.

A. Spectrum and first-order perturbation theory of the ground state

In this section we discuss some features of the raw spectrum of the Hubbard model. Only later in Sec. VI are we going to unfold the spectrum and look for universal features. As a function of the coupling strength U/t the spectrum clearly falls into three classes. In the weak-coupling limit $(U/t\ll W/t)$, to be studied in more detail below, the spectrum acquires a band width $W\approx32t$. It consists of a number M of well-separated minibands reminiscent of the huge degeneracy at zero coupling due to size quantization. For intermediate-coupling strengths $(U/t\approx W/t)$ the spectrum becomes rather featureless. No apparent gaps or bands emerge. In the strong-coupling limit $(U/t\gg W/t)$ the spectrum splits up into three well-separated bands centered around the energies $E/t=0,U/t,2U/t$. These are the Hubbard bands corresponding to states containing zero, one, or two pairs of electrons. In Fig. 4 are shown one typical spectrum from each of the three coupling strength regimes.

We now focus on the weak-coupling limit where it is natural to make Fourier transforms from real space to momentum space, $\hat{c}_{\mathbf{k}\sigma}^\dagger\equiv(1/L)\Sigma_j\exp(i\mathbf{k}\cdot\mathbf{r}_j)\hat{c}_{j\sigma}^\dagger$, where $\mathbf{k}=(k^x,k^y)$, with $k^\xi=2\pi n/L$ and $n=0,1,\ldots,L-1$. The eigenstates of the kinetic energy operator $-t\hat{T}$ are

$$|\mathbf{k}_0,\mathbf{k}_1;\mathbf{k}_2,\mathbf{k}_3\rangle=\hat{c}_{\mathbf{k}_1\uparrow}^\dagger\hat{c}_{\mathbf{k}_2\uparrow}^\dagger\hat{c}_{\mathbf{k}_3\downarrow}^\dagger\hat{c}_{\mathbf{k}_3\downarrow}^\dagger|\mathrm{vac}\rangle,$$

$$-t\hat{T}|\mathbf{k}_0,\mathbf{k}_1;\mathbf{k}_2,\mathbf{k}_3\rangle=-2t\sum_{n=0}^{3}E(\mathbf{k}_n)|\mathbf{k}_0,\mathbf{k}_1;\mathbf{k}_2,\mathbf{k}_3\rangle, \quad (26)$$

$$E(\mathbf{k}_n)=\cos(k_n^x)+\cos(k_n^y).$$

The Pauli principle prevents $\mathbf{k}_0=\mathbf{k}_1$ and $\mathbf{k}_2=\mathbf{k}_3$, and the ground-state energy $E_L^{(0)}$ becomes

$$E_L^{(0)}=-12t-4t\cos(2\pi/L). \quad (27)$$

For large lattices this tends toward $-16t$ and results in a bandwidth $W=32t$. For $L=3$, 4, 5, and 6, respectively, the

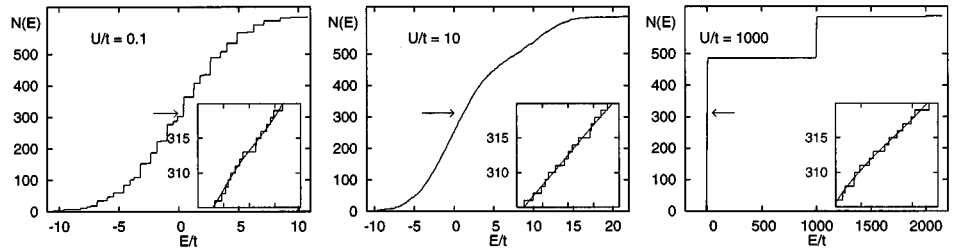

FIG. 4. The integrated density of states $N(E)$ of the Hubbard model with four electrons on the 5×5 lattice for the irreducible representation $(R,S)=(10,0)$ with $U/t=0.1,10,1000$. For $U/t=0.1$ the minibands are still clearly visible and $N(E)$ is essentially featureless for $U/t=10$, while for $U/t=1000$ the three Hubbard bands at 0, 1000, and 2000 appear. The insets are magnifications of $N(E)$ where the arrows point. The smooth $\bar{N}(E)$ is added.

actual bandwidths W/t are 20.0, 24.0, 26.2, and 28.0 while the number M of minibands for $U=0$ are 7, 13, 42, and 29.

The limitation of perturbation theory is demonstrated by a first-order degenerate perturbation calculation for the ground state. Let p_L be the one-dimensional momentum component $p_L=2\pi/L$ and construct the 5 two-dimensional momentum vectors $\mathbf{0}=(0,0)$, $\mathbf{q}^0=(p_L,0)$, $\mathbf{q}^1=(0,p_L)$, $\mathbf{q}^2=(-p_L,0)$, and $\mathbf{q}^3=(0,-p_L)$. The 16 states $|\mu,\lambda\rangle$, defined as

$$|\mu,\lambda\rangle=|\mathbf{0}_\uparrow,\mathbf{q}^\mu_\uparrow;\mathbf{0}_\downarrow,\mathbf{q}^\lambda_\downarrow\rangle,\quad \mu,\lambda=0,1,2,3, \tag{28}$$

form the ground-state multiplet separated from the next multiplet by an energy gap $\Delta E_L=2t[1-\cos(p_L)]$. In momentum space the interaction operator $U\hat{U}$ takes the form

$$U\hat{U}=\frac{U}{L^2}\sum_{\mathbf{k}_1,\mathbf{k}_2,\mathbf{q}}\hat{c}^\dagger_{\mathbf{k}_1+\mathbf{q}\uparrow}\hat{c}_{\mathbf{k}_1\uparrow}\hat{c}^\dagger_{\mathbf{k}_2-\mathbf{q}\downarrow}\hat{c}_{\mathbf{k}_2\downarrow}, \tag{29}$$

and after some simple algebra the matrix elements of the perturbation are found to be

$$\langle m,l|U\hat{U}|\mu,\lambda\rangle=\frac{U}{L^2}(3\delta_{m,\mu}\delta_{l,\lambda}+\delta_{m+l,\mu+\lambda}). \tag{30}$$

The eigenvalues can be found analytically, and we end up with the following expression for the perturbed levels $E^{(1)}_{L,\beta}(U)$ with degeneracies d:

$$E^{(1)}_{L,\beta}(U)=E^{(0)}_L+\beta\frac{U}{L^2},\quad \beta=3_{(d=7)},4_{(d=4)},5_{(d=4)},7_{(d=1)}. \tag{31}$$

Thus in first-order perturbation theory the ground-state degeneracy is partly lifted, leaving a sevenfold-degenerate ground state for $U>0$.

In Fig. 5 we compare the exact numerical calculation with Eq. (31) for $L=5$ and 6. Note especially how in the exact calculation the degeneracy of the ground-state energy is lifted completely. This is also demonstrated in Table II, where it can be seen that also for $L=3$ the ground state is nondegenerate. However, the ground state of $L=4$ remains threefold degenerated even in the exact calculation. This reflects the particular symmetry of the 4×4 lattice, where the hyperplane reflection r_h leads to the existence of threefold-degenerate representations as shown in Appendix A.

Using the quantum numbers (k_x,k_y,b_x,b_y,c) of Table V in Appendix B to interpret the representation label R in Table II we note that they are of the same form for $L=3,5,6$: $(0,0,1,1,-1)$, $(0,0,1,-1,*)$, $(2\pi/L,2/\pi/L,*,*,-1)$, $(4\pi/L,0,*,1,*)$, $(2\pi/L,2\pi/L,*,*,1)$, and $(0,0,1,1,1)$, where the first set corresponds to the unique ground state. This result extends to the $L=4$ lattice when the actual space group is replaced by the one generated by $\{t_x,r_x,t_y,r_y,r_d\}$. One state in the $L=4$ triplet ground state belongs to the $(0,0,1,1,-1)$ representation and the other two states to $(4\pi/L,0,1,1,*)$. In all cases the ground state is odd with respect to the diagonal reflection r_d, which is understandable since that symmetry suppresses the ability of having pairs along the diagonal. Finally we note that due to the aforementioned spin symmetry of the Hubbard model, the ground state of the $S_z=0$ sector is in fact a global ground state, and furthermore since it has $S=0$, the same energy level does not exist in any other S_z sector. Thus we can conclude that the global ground state in the generic case $(L\neq4)$ is nondegenerate.

B. Remaining degeneracies

After taking all the known symmetries into account and after projecting into the symmetry-invariant subspaces, it

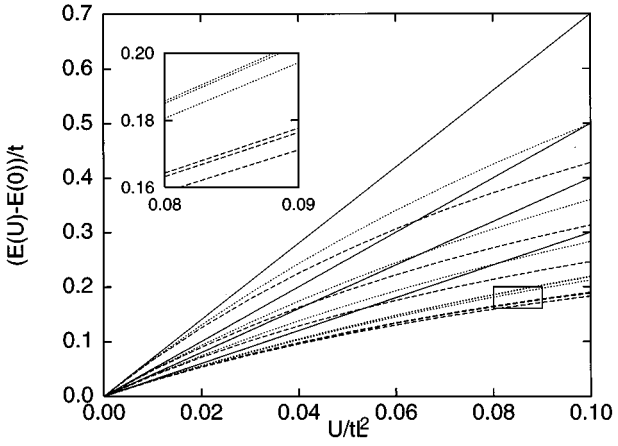

FIG. 5. The evolution of the 16-fold degenerated ground state multiplet as a function of U/L^2. The exact numerical results for $L=5$ (dotted lines) and $L=6$ (dashed lines) are contrasted with the first-order perturbation calculation (solid straight lines). The inset is a magnification of that portion of the plot marked by a rectangle, showing how the exact calculation leads to a splitting into three submultiplets with degeneracies 1, 2, and 4 of the sevenfold-degenerate perturbation theory ground state. The exact ground state is nondegenerate. See also Table II.

TABLE II. For $U/tL^2=0.02$ the sevenfold-degenerate perturbation theory ground state $E^{(1)}_{L,\beta=3}$ given in row P is compared with the exact energies E of the 16 levels splitting off from the $U=0$ ground state $E^{(0)}_L$ The degeneracies of the submultiplets are given by the dimension l_R of the corresponding irreducible representation R of the space group. Note that except for $L=4$ the exact ground state is nondegenerate. Also listed are the quantum numbers (R,S,J) of the levels.

	$L=3$		$L=4$		$L=5$		$L=6$	
No.	E/t	$(R,S)l_R$	E/t	$(R,S,J)l_R$,	E/t	$(R,S)l_R$	E/t	$(R,S,J)l_R$
P	−9.94000	(−,−) 7	−11.94000	(−,−,−) 7	−13.17607)	(−,−) 7	−13.94000	(−,−,−) 7
0	−9.94122	(2,0) 1	−11.94268	(9,0,6) 3	−13.18059	(2,0) 1	−13.94676	(4,0,16) 1
1	−9.94110	(8,1) 4	−11.94232	(16,1,6) 6	−13.18012	(4,1) 2	−13.94617	(9,1,16) 2
2	−9.94097	(4,1) 2	−11.90425	(17,0,6) 6	−13.18005	(10,1) 4	−13.94606	(25,1,16) 4
3	−9.92188	(5,0) 4	−11.86560	(0,0,6) 1	−13.16204	(7,0) 4	−13.92870	(14,0,16) 4
4	−9.90229	(7,0) 4		–	−13.14302	(9,0) 4	−13.91032	(24,0,16) 4
5	−9.86204	(0,0) 1		–	−13.10590	(0,0) 1	−13.87494	(0,0,16) 1

turns out that within each subspace some further degeneracies remain. The reason is that the low filling of the lattice allows for a kind of restricted permutation symmetry for the particle momentum components, resulting in energy eigenstates which are simultaneously eigenstates of $\hat{T}$ and $\hat{U}$ and therefore independent of U (though their eigenvalues might depend on U). We denote such states $\hat{T}/\hat{U}$ states or $|\psi^{\gamma}_{S}\rangle$, where S is the spin and γ the eigenvalue of $\hat{U}$. With four electrons γ takes the values $\gamma=0,1,2$ corresponding to a superposition of states containing exactly γ pairs, i.e., doubly occupied sites. A generic energy eigenstate is not a $\hat{T}/\hat{U}$ state and in that case we write $\gamma=*$. In Table III we show the number of generic energy eigenstates and $\hat{T}/\hat{U}$ states found numerically. The Hubbard model is thus partly integrable. The spectrum of each symmetry-invariant subspace is a mixture of an integrable component (the $\hat{T}/\hat{U}$ states) and a nonintegrable component (the generic states), and in the analysis in Sec. VI of the spectral statistics we throw away the integrable component and analyze only the generic nonintegrable component.

The $\hat{T}/\hat{U}$ states are formed by specific superpositions of eigenstates of $\hat{T}$ by permuting the eight momentum components k^{ζ}_n $\zeta=x,y$ and $n=0$, 1, 2, and 3, such that the sum of cosines in Eq. (26) remains unchanged. In the following we mention some large classes of such states. The reader is referred to Appendix D for details.

First we note that for even L proportionally many more states remain degenerate as compared to L odd. This difference is due to the momentum component $k^{\zeta}_n=\pi$, which only exists for L even. Because $\cos(\pi-k)+\cos(k)=0$ independent of k, such terms drop out when $\hat{T}$ is applied to a state containing this combination and a certain degree of freedom is left to form the $\hat{T}/\hat{U}$ state superpositions. Starting with two-pair states $\gamma=2$ we find exactly one energy eigenstate

TABLE III. For $L=3$, 4, 5, and 6 is shown the number of energy eigenstates found numerically in each of the four main groups indexed by γ. The first group, denoted $\gamma=*$, contains the generic energy eigenstates that are not eigenstates of $\hat{U}$. The three other groups, denoted $\gamma=0,1,2$, respectively, contain the nongeneric $\hat{T}/\hat{U}$ states that are simultaneous eigenstates of $\hat{U}$ (with eigenvalue γ) and $\hat{T}$. In parentheses are given the number of states that remain degenerated in the symmetry-invariant subspaces after taking the space, spin, and pseudospin symmetries into account. Note how the $\gamma=*$ states exhibit no further degeneracy. In the last row denoted ''%'' are given the percentages of $\gamma=*$ states out of the total number of states.

γ	S	$L=3$	$L=4$	$L=5$	$L=6$
*	0	540/(0)	4169/(0)	31977/(0)	115896/(0)
*	1	621/(0)	4472/(0)	41662/(0)	137199/(0)
*	2	0/(0)	0/(0)	0/(0)	0/(0)
0	0	0/(0)	1176/(1143)	523/(316)	23555/(23427)
0	1	9/(0)	2548/(2519)	3188/(2823)	60306/(60160)
0	2	126/(80)	1820/(1727)	12650/(12362)	58905/(58723)
1	0	0/(0)	94/(14)	0/(0)	408/(247)
1	1	0/(0)	120/(24)	0/(0)	630/(420)
1	2	0/(0)	0/(0)	0/(0)	0/(0)
2	0	0/(0)	1/(0)	0/(0)	1/(0)
2	1	0/(0)	0/(0)	0/(0)	0/(0)
2	2	0/(0)	0/(0)	0/(0)	0/(0)
%		89.6%	60.0%	81.8%	63.8%

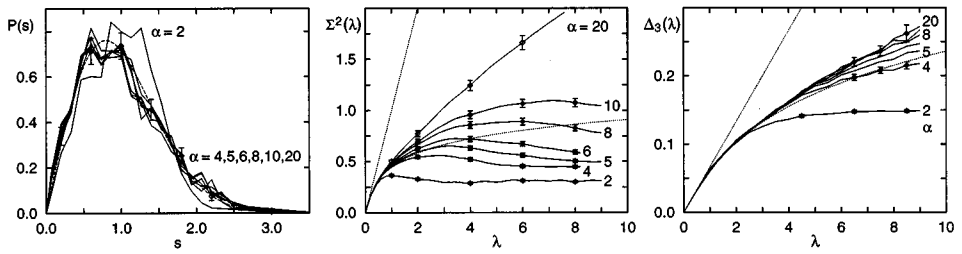

FIG. 6. The spectral statistics $P(s)$, $\Delta_3(\lambda)$, and $\Sigma^2(\lambda)$ for the invariant subspace $(R,S)=(13,1)$ of the 5×5 lattice as a function of the free parameter α of the unfolding procedure using Gaussian broadening with variable width. In all three panels the values for α are 2, 4, 5, 6, 8, 10, and 20. In the first panel six of the seven curves fluctuate around $P^{\mathrm{GOE}}(s)$, hardly visible as a smooth dotted line. In the two other panels the Poisson case is given as a dotted straight line while the GOE case is given by a dotted smooth curve. For all data sets a few representative error bars are shown.

$|\psi_{S=0}^{\gamma=2}\rangle$. It depends on the momentum π, and hence it exits only for even L. Similarly, for one-pair states only even L leads to $\hat{T}/\hat{U}$ states. A number $\binom{L^2}{2}$ of states $|\psi_{S=1}^{\gamma=1}\rangle$ can easily be constructed. More care must be taken upon forming the corresponding $S=0$ states. However, we have succeeded in constructing analytically the number of states $|\psi_{S=0}^{\gamma=1}\rangle$ required by Table III. Finally, for zero-pair states the existence of the momentum π is not required to form the $\hat{T}/\hat{U}$ states, but it certainly helps. Thus both even and odd values of L lead to nongeneric energy eigenstates, but relatively more such states are found for even L. It is easy to see that all states with the maximal spin $S=2$ are $\hat{T}/\hat{U}$ states $|\psi_{S=2}^{\gamma=0}\rangle$. This is a trivial consequence of choosing four different sites (or momenta) and forming the superposition given in Eq. (13). There are $\binom{L^2}{4}$ such states. The construction of states $|\psi_{S=S'}^{\gamma=0}\rangle$ with $S'=1$ or 0 is more cumbersome, and so in Appendix D we have only given two examples of classes of such states.

The main result of this section is that the degeneracies that remain after space, spin, and pseudospin symmetry have been taking into account is related to a restricted permutation symmetry of the momentum components. We have not found the associated projection operators, but numerically and partly analytically we have established the fact that the degenerate states are simultaneously eigenstates of $\hat{T}$ and $\hat{U}$ with energies $E(U)=E(0)+\gamma U$. By discarding these states we end up with nondegenerate $\hat{U}$-dependent states. It is the spectral statistics of these states we analyze in the following section, and this analysis confirms our claim that all symmetries indeed have been taken into account.

VI. SPECTRAL STATISTICS OF THE HUBBARD MODEL

Having sorted the spectrum according to all symmetries including the restricted permutation symmetry of the momentum components the RMT analysis can be performed. As discussed in Sec. III the first step is the unfolding of the spectrum. There we mentioned how the unfolding procedure is not uniquely determined, and so we turn to that problem first.

A. Optimization of the unfolding procedure

We unfold the spectra by using the method of Gaussian broadening with variable width discussed in Sec. III A. The question now arises as to how to choose the free parameter α corresponding to how many energy levels each Gaussian essentially spreads out over to each side. The problem we face is illustrated in Fig. 6 where it is seen that although the level spacing distribution $P(s)$ is essentially independent of the choice of α, both the number variance $\Sigma^2(\lambda)$ and the spectral rigidity $\Delta_3(\lambda)$ vary with α. It is seen that $\Delta_3(\lambda)$ is less sensitive to changes in α than $\Sigma^2(\lambda)$. The former seems to saturate for large values of α, while the latter continues to grow rapidly as α enhances. We have chosen that value α_0 of α which makes $\Sigma^2(\lambda)$ fit the corresponding GOE curve as well as it can. In general that leads to $\alpha_0\approx4$. We note that for this choice of α, $\Delta_3(\lambda)$ is almost saturated, while $P(s)$ remains unchanged. Thus, two of the three statistics are essentially independent of variations of α around α_0, while the third is as close to the GOE behavior as it can be.

To illustrate the importance of sorting the spectrum by group theory we show in Fig. 7 the level spacing distribution for $L=4$ with $U/t=10$ for the case where all symmetries are taken into account (''full symm.'') and for the case with lower symmetry (''low symm.'') where the spin and pseudospin symmetries are being kept intact but where the space group has been reduced by replacing among the generators

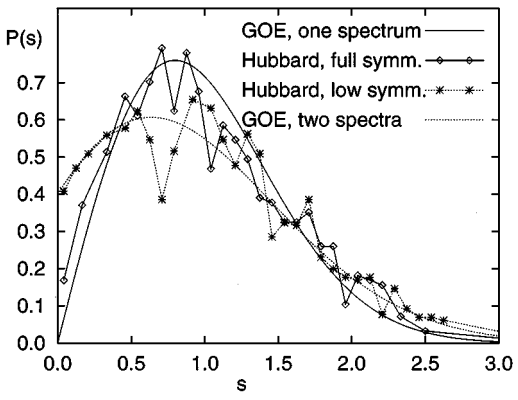

FIG. 7. $P(s)$ for $L=4$ with $U/t=10$ is calculated after sorting the spectra using either the full symmetry group of the Hamiltonian ($\diamond$) or an symmetry group artificially lowered (*) as described in the text. The full symmetry case compares well with the Wigner surmise (smooth solid curve) whereas the lower-symmetry case compares well with the distribution of two GOE spectra mixed with relative weights 0.72 and 0.28 (dotted smooth curve).

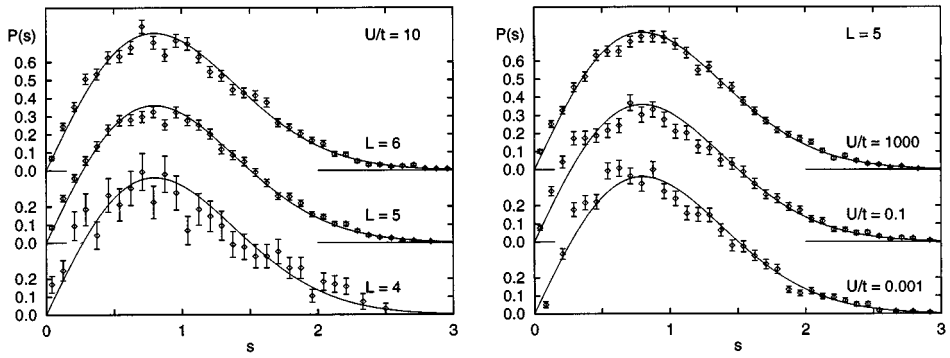

FIG. 8. The probability distribution $P(s)$ of the level spacings s averaged over the largest symmetry-invariant subspaces for the Hubbard model with four electrons on square $L\times L$ lattices. To the left is shown $P(s)$ as a function of lattice size L at medium-coupling strength. The data represent $L=4$, 5, and 6 for $U/t=10.0$. To the right is shown $P(s)$ as a function of coupling strength at fixed low filling. The data represent $U/t=0.1$, 10, and 1000 for $L=5$. The solid line is the Wigner distribution found for GOE random matrices.

the special hyperplane reflection r_h with the ordinary diagonal reflection r_d. For the full symmetry case a distribution rather close to the Wigner surmise is found, whereas the level repulsion is partially lost for the low-symmetry case, and the data fit reasonably well the distribution found by mixing two GOE spectra[21] with relative weights 0.72 and 0.28. This makes sense since by lowering the symmetry group artificially, spectra from the independent true symmetry-invariant subspaces are being mixed. For the more severe symmetry reduction where the pseudospin is altogether neglected and the space group is generated only by $\{t_x,t_y\}$, we find the level spacing distribution to be the Poisson (exponential) distribution (not shown in the figure).

B. Statistics $P(S)$, $\Sigma^2(\lambda)$, and $\Delta_3(\lambda)$ of the Hubbard model

In this subsection we present the results of the spectral statistical analysis of the Hubbard model at low filling. We present only results for $L=4$, 5, and 6 since $L=3$ yields too poor statistics due to its small invariant subspaces. Besides letting L vary we are also varying the coupling strength U/t and present results for weak-, intermediate-, and strong-coupling regimes for $L=5$. To improve on the statistics we have averaged over the largest invariant subspaces. For $P(s)$ the sizes δP of the error bars shown in the figures are estimated by $\delta P_i=C\sqrt{n_i}/h_i$, where n_i is the number of points in bin i of the associated histogram and h_i is the width of the bin, while C is the normalization factor rendering a total probability of 1. For $\Sigma^2(\lambda)$ and $\Delta_3(\lambda)$ the error bars are estimated by ordinary variances obtained from the values calculated in the many contiguous intervals of length λ throughout the unfolded spectrum.

The results for $P(s)$ are shown in Fig. 8. It is seen that for all lattice sizes and for any value of the coupling strength the level spacing distribution is fairly close to the Wigner distribution of the GOE; it possesses a pronounced linear level repulsion for small s, a peak near $s=0.8$, signaling spectral rigidity, and a rapid falloff for $s>2$.

In Fig. 9 is shown $\Sigma^2(\lambda)$ of the Hubbard model for the same parameters as for $P(s)$ just mentioned. When λ is small the rigidity of the Hubbard spectrum is very close to that of the GOE random matrices, while for larger λ a saturation sets in. For all values of U/t we find the critical value λ^* where the departure from the GOE sets in to be roughly 2. The precise origin of λ^* remains unclear.

Finally, in Fig. 10 are shown the results for the spectral rigidity $\Delta_3(\lambda)$. As $\Sigma^2(\lambda)$ also $\Delta_3(\lambda)$ displays an excellent agreement with the GOE for $\lambda<\lambda^*\approx 2$, for all fillings and for all values of U/t. The deviations from the GOE beyond λ^* are not so marked. The curves lie between the Poisson line and the GOE curve, but rather close to the latter.

It is remarkable how the results for the three statistics studied are fairly independent of the size of the lattice (equivalent to the filling) and of the coupling strength. We find GOE-like behavior not only for all finite values of U/t including those close to the integrable $U=0$ limit, but also for filling factors as low as 0.06 close to the integrable single-particle limit. However, as is evident from the behavior of especially $\Sigma^2(\lambda)$ at large energy scales, the Hubbard model cannot be modeled exactly by a simple GOE random matrix model.

VII. CONCLUSIONS AND DISCUSSION

In this paper the energy level statistics of the Hubbard model for $L\times L$ square lattices ($L=3,4,5,6$) at low filling (four electrons) has been studied numerically for a wide range of the coupling strength. With great care all known symmetries of the model (space, spin, and pseudospin symmetry) have been taken into account explicitly from the beginning of the calculation by projecting into symmetry-invariant subspaces. The details of this group theoretical treatment were presented with special attention to the nongeneric case of $L=4$, where a particular complicated space group appears. The resulting reduction of the numerical diagonalization is significant, and the method presented can in a straightforward manner be extended to larger lattices and higher fillings and thus form the basis of improved numerical studies of the Hubbard model and related models without disorder. In particular, this work can be used as a starting point for calculating various spectral functions, for which explicit forms of the eigenstates are required. This will be dealt with in forthcoming work.

For all the lattices studied a significant amount of levels

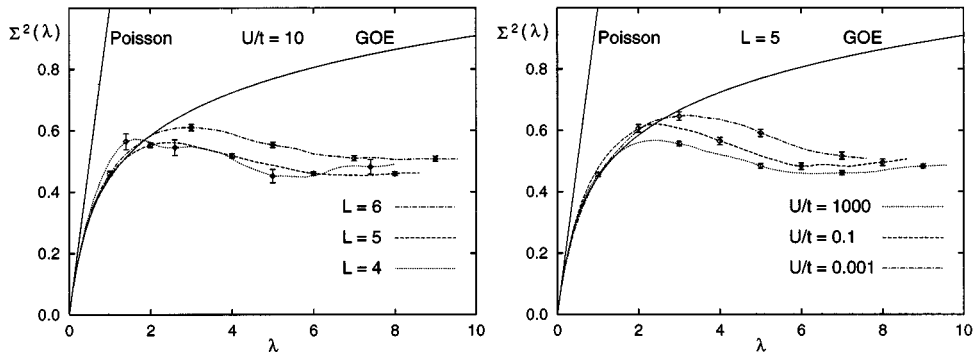

FIG. 9. The number variance $\Sigma^2(\lambda)$ calculated for the same parameters as in Fig. 8. The data are compared to the results of the random diagonal matrix ensemble (Poisson) and the random full matrix ensemble (GOE), shown as the straight solid line and the curved solid line, respectively.

within each symmetry-invariant subspace remain degenerated, but except for $L=4$ the ground state is nondegenerate. We explained the degenerate states as a consequence of a restricted permutation symmetry of the momentum components. These states, all independent of U, form an integrable part of the spectrum, and after discarding them we end up with nondegenerate spectra on which the level statistical analysis could be performed.

The intricate structure of the Hubbard spectra necessitated the development of a careful unfolding procedure as a preparatory step before the level statistical analysis. The procedure we arrived at tested favorably in many cases of pathological spectra, and it seems to be very robust and applicable in general cases were no other natural unfolding procedure exists.

Finally, we have performed a level statistical analysis of the Hubbard spectra, and we presented results for the level spacing distribution $P(s)$, the number variance $\Sigma^2(\lambda)$, and the spectral rigidity $\Delta_3(\lambda)$. The statistics for the different lattice sizes and for a wide range of coupling strengths are essentially the same: $P(s)$ shows good agreement with the GOE. $\Sigma^2(\lambda)$ agrees only with the GOE up to the U/t-independent medium-sized energy scale $\lambda^*\approx 2$ beyond which a saturation sets in. $\Delta_3(\lambda)$ also agrees with the GOE for $\lambda<\lambda^*$. The deviation from the GOE beyond λ^* is not so marked as that for $\Sigma^2(\lambda)$. The curve falls between that of the GOE and the Poissonian case, but rather close to the former. We stress that these results were also obtained for very small coupling strengths approaching the integrable zero-coupling limit. This emphasizes the nonperturbative nature of the model revealed by our analysis: Even the smallest deviation from the integrable limits leads to spectral statistics usually associated with nonintegrability and quantum chaos, and in this sense the model seems always to be in the strong-coupling limit.

Largely, our results show GOE behavior of the spectral statistics of the typical high-lying excitations of the Hubbard model at low filling. This indicates that at least the incoherent part of the electronic spectral functions (related to the coherent part describing the low-lying electronic excitations through sum rules) is out of reach by standard methods. On the other hand, it should be possible to model this part by a random matrix ansatz. This is in agreement with previous results of the t-J model near half filling.[15] However, the cause of the deviations from the GOE we found in $\Sigma^2(\lambda)$ and $\Delta_3(\lambda)$ beyond λ^* remains an open question. A similar question has been answered in general for single-particle systems with mean-level spacing Δ: In disordered (metallic) systems $\lambda^*\Delta\sim\hbar/\tau_D$, where τ_D is the time it takes a particle to diffuse through the system,[34] whereas for pure (ballistic) systems $\lambda^*\Delta\sim\hbar/\tau_0$, where τ_0 is the period of the shortest periodic orbit.[35] Results are also beginning to emerge for disordered interacting lattice systems, where λ^* is related to the ratio U/W between some interaction strength U and the disorder-induced single-particle bandwidth W.[16,36] For these systems the deviations from the GOE are due to the preferential basis supplied by the given disorder potential. For example, the system consisting of two interacting particles in a disorder potential[36] could be studied analytically by adding a random diagonal matrix modeling the disorder single-particle states to a random GOE matrix modeling the interactions between these states, and it was found that $\Sigma^2(\lambda)$ increased as a power law for $\lambda>\lambda^*$. This behavior is in contrast to the saturation we found (see Fig. 9), which looks more like the result of the ballistic single-particle case.[35] It is perhaps not surprising that such a similarity exists between

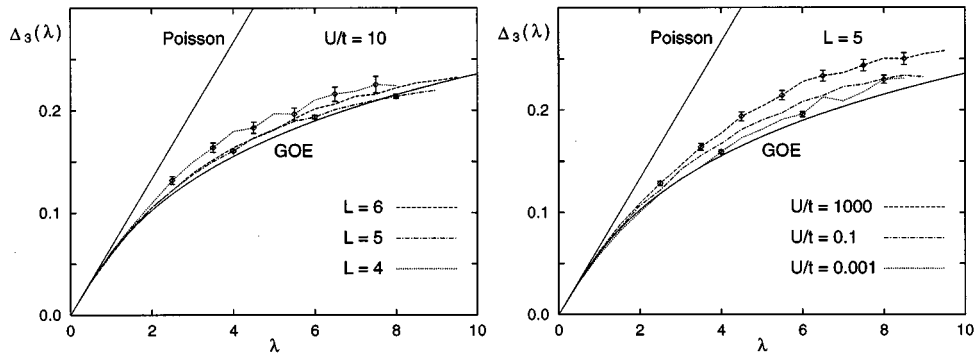

FIG. 10. The spectral rigidity $\Delta_3(\lambda)$ calculated for the same parameters as in Fig. 8. The data are compared to the results of the random diagonal matrix ensemble (Poisson) and the random full matrix ensemble (GOE), shown as the straight solid line and the curved solid line, respectively.

the disorder-free chaotic single-particle case and the disorder-free Hubbard model rather than between two strongly correlated systems one with and the other without disorder. However, exactly what physical mechanism produces a preferential basis for the Hubbard model at low filling is not known, and neither is it known why a similar mechanism is suppressed for the t-J model near half filling, where much less pronounced deviations from the GOE are found.[15] These questions are topics for future work.

ACKNOWLEDGMENTS

It is a pleasure to thank Benoit Douçot, Jean-Louis Pichard, Clément Sire, and Dietmar Weinmann for stimulating discussions and Elliot H. Lieb for valuable comments. We thank the Centre Grenoblois de Calcul Vectoriel for its kind help with the part of our numerical work that was carried out at its CRAY-94 computer. H.B. was supported by the European Commission under Grant No. ERBFMBICT 950414.

APPENDIX A: THE IRREDUCIBLE REPRESENTATIONS OF G_4

In Sec. IVA we showed how the group G_4 of the neighbor-conserving transformation of the 4×4 lattice is isomorphic with the point group of the four-dimensional hypercube. In this appendix we determine the structure of this group and we sketch how the irreducible representations are found analytically. The fundamental simplification is the observation that G_4 has the structure of a semidirect product involving an invariant Abelian subgroup. The theorem of induced representations[24] can then be used to find all irreducible representations. The theorem is stated below. The coordinate set of a corner in the unit hypercube in four dimensions is given as a 4 bit binary number. Any transformation of the hypercube can thus be written as a permutation of the 4 bits followed by bit inversion ($0\leftrightarrow1$) of all, some, or none of the bits.

In what follows any quadruple (x_1,x_2,x_3,x_4) is written in shorthand notation as (x_i). The group of bit permutations is of course the permutation group S_4 denoted $\mathcal{B}$ in the following to be consistent with Ref. 24, on which the group theoretical work in this appendix is based. Any element $b\in\mathcal{B}$ is written as $b=(b_i)=(b_1,b_2,b_3,b_4)$, listing the permutation of the numbers 1, 2, 3, and 4. The group of bit inversions is denoted $\mathcal{A}$. It is easily seen that $\mathcal{A}=\mathcal{Z}_2\otimes\mathcal{Z}_2\otimes\mathcal{Z}_2\otimes\mathcal{Z}_2$, since bit inversions do or do not take place on each of the 4 bit positions. Any element $a\in\mathcal{A}$ has the form $a=(a_i)=(a_1,a_2,a_3,a_4)$, with $a_i=\pm1$, where $+1$ means no bit inversion and -1 means bit inversion. Any element of $g\in G_4$ can be written as $g=ab=(a_ib_i)$ and conversely all products $ab\in G_4$. $\mathcal{A}$ contains 16 elements and $\mathcal{B}$ contains 24 so that G_4 contains 384 elements. It is readily verified that $\mathcal{A}$ is an Abelian subgroup of G_4. Furthermore, $\mathcal{A}$ is an invariant subgroup since for $\forall a\in\mathcal{A},\forall b\in\mathcal{B}$: $bab^{-1}=b(a_i)b^{-1}=(a_{b(i)})bb^{-1}=(a_{b(i)})\in\mathcal{A}$. Finally, the only common element of $\mathcal{A}$ and $\mathcal{B}$ is the identity. We can therefore conclude that G_4 is a semidirect product of the invariant Abelian subgroup $\mathcal{A}$ with $\mathcal{B}$:

$$G_4=\mathcal{A}\circledS\mathcal{B}=(\mathcal{Z}_2\otimes\mathcal{Z}_2\otimes\mathcal{Z}_2\otimes\mathcal{Z}_2)\circledS S_4. \tag{A1}$$

The first step in calculating the irreducible representations for G_4 is to construct the character table $\chi^{\mathbf{q}}(a)$ of $\mathcal{A}$. This is easily found as the product of the character table

$$\begin{vmatrix} 1 & 1 \\ 1 & -1 \end{vmatrix}$$

for $\mathcal{Z}_2$ with itself 4 times. The 16 irreducible representations are identified by the index $\mathbf{q}=(q_1,q_2,q_3,q_4)$, with $q_i=0$ or 1, and the $\mathbf{q}$th character $\chi^{\mathbf{q}}(a)$ is given by the product of a_i to the power q_i:

$$\chi^{\mathbf{q}}(a)=\prod_{i=1}^{4}a_i^{q_i}. \tag{A2}$$

Next step is to pick any $\mathbf{q}'$ and construct the associated little group $\mathcal{B}(\mathbf{q}')\subseteq\mathcal{B}$ defined as

$$\mathcal{B}(\mathbf{q}')\equiv\{b\in\mathcal{B}|\chi^{\mathbf{q}'}(bab^{-1})=\chi^{\mathbf{q}'}(a),\ \text{for}\ \forall a\in\mathcal{A}\}. \tag{A3}$$

The group $\mathcal{B}$ is then written in a coset decomposition after $\mathcal{B}(\mathbf{q}')$:

$$\mathcal{B}=\mathcal{B}(\mathbf{q}')b_1\oplus\mathcal{B}(\mathbf{q}')b_2\oplus\cdots\oplus\mathcal{B}(\mathbf{q}')b_{M'}. \tag{A4}$$

For each of the M' coset representatives b_j an index $\mathbf{q}'_j$ is determined such that

$$\chi^{\mathbf{q}'_j}=\chi^{\mathbf{q}'}(b_jab_j^{-1}),\quad \text{for}\ \forall a\in\mathcal{A}. \tag{A5}$$

Note that b_1 is the identity and that $\mathbf{q}'_1$ hence equals $\mathbf{q}'$. The set $\mathrm{orb}(\mathbf{q}')=\{\mathbf{q}'_1,\mathbf{q}'_2,\ldots,\mathbf{q}'_{M'}\}$ is called the orbit of $\mathbf{q}'$. Now pick a $\mathbf{q}''$ outside $\mathrm{orb}(\mathbf{q}')$ and repeat the procedure. This is continued until each of the 16 $\mathbf{q}$'s are associated with an orbit. The last thing to do before constructing the irreducible representations of G_4 is to find the irreducible representations $\Delta^{\mathbf{q}'p}$ of the little group $\mathcal{B}(\mathbf{q}')$. This is usually a simple step due to the small size of $\mathcal{B}(\mathbf{q}')$.

The theorem of induced representations[24] states that all irreducible representations $\Gamma^{\mathbf{q}'p}$ of the semidirect product $\mathcal{A}\circledS\mathcal{B}$, $\mathcal{A}$ being an invariant Abelian subgroup, are found as follows. (i) Pick one $\mathbf{q}'$ from each orbit. (ii) Construct the little group $\mathcal{B}(\mathbf{q}')$ and its n'_p irreducible representations $\Delta^{\mathbf{q}'p}$, $p=1,\ldots,n'_p$. (iii) Find the M' coset representatives $b_j\in\mathcal{B},j=1,\ldots,M'$, of $\mathcal{B}$ with respect to $\mathcal{B}(\mathbf{q}')$. (iv) Then the matrix elements of $\Gamma^{\mathbf{q}'p}$ for element ab are given by

$$\Gamma^{\mathbf{q}'p}(ab)_{kt,jr}=\begin{cases}\chi^{\mathbf{q}'}(a)[\Delta^{\mathbf{q}'p}(b_kbb_j^{-1})]_{\mathrm{tr}} & \text{if}\ b_kbb_j^{-1}\in\mathcal{B}(\mathbf{q}'),\\ 0 & \text{if}\ b_kbb_j^{-1}\notin\mathcal{B}(\mathbf{q}').\end{cases} \tag{A6}$$

Here we will not give the explicit expressions of the irreducible representations of G_4, but rather just briefly sketch the construction of them and calculate how many there are and what is the dimension of each of them.

First we chose $\mathbf{q}'=(0000)$. From Eq. (A2) it is easily seen that $\chi^{(0000)}(a)=1$ for $\forall a\in\mathcal{A}$. Hence $\chi^{(0000)}(bab^{-1})=\chi^{(0000)}(a)$ for $\forall a\in\mathcal{A}$, $\forall b\in\mathcal{B}$, and according to Eq. (A3) we find $\mathcal{B}(0000)=\mathcal{B}$. The coset representation of $\mathcal{B}$ consists of only one term and the single coset representative b_1 is the identity. As a consequence we have $\mathrm{orb}(0000)=\{(0000)\}$. Finally, the irreducible representa-

TABLE IV. The character table of G_4 defining the index R for each of the 20 irreducible representations and the index C for each of the 20 classes. Column $C=0$ contains the dimension l_R ranging from 1 to 8 of the representations.

$R\backslash C$	0	1	2	3	4	5	6	7	8	9	10	11	12	13	14	15	16	17	18	19
0	1	1	1	1	1	1	1	1	1	1	1	1	1	1	1	1	1	1	1	1
1	1	1	1	1	1	1	1	1	1	1	1	−1	−1	−1	−1	−1	−1	−1	−1	−1
2	1	1	1	1	1	1	1	−1	−1	−1	−1	1	1	1	1	−1	−1	−1	−1	−1
3	1	1	1	1	1	1	1	−1	−1	−1	−1	−1	−1	−1	−1	1	1	1	1	1
4	2	2	2	2	2	−1	−1	0	0	0	0	0	0	0	0	1	1	−2	−2	−2
5	2	2	2	2	2	−1	−1	0	0	0	0	0	0	0	0	−1	−1	2	2	2
6	3	3	−1	3	−1	0	0	1	1	−1	1	−1	−1	1	−1	0	0	1	−3	−3
7	3	3	−1	3	−1	0	0	−1	−1	1	−1	1	1	−1	1	0	0	1	−3	−3
8	3	3	−1	3	−1	0	0	−1	−1	1	−1	−1	−1	1	−1	0	0	−1	3	3
9	3	3	−1	3	−1	0	0	1	1	−1	1	1	1	−1	1	0	0	−1	3	3
10	4	−4	0	0	0	1	−1	−2	2	0	0	2	−2	0	0	−1	1	0	−2	2
11	4	−4	0	0	0	1	−1	2	−2	0	0	−2	2	0	0	−1	1	0	−2	2
12	4	−4	0	0	0	1	−1	2	−2	0	0	2	−2	0	0	1	−1	0	2	−2
13	4	−4	0	0	0	1	−1	−2	2	0	0	−2	2	0	0	1	−1	0	2	−2
14	6	6	2	−2	−2	0	0	0	0	0	0	−2	−2	0	2	0	0	0	0	0
15	6	6	−2	−2	2	0	0	−2	−2	0	2	0	0	0	0	0	0	0	0	0
16	6	6	−2	−2	2	0	0	2	2	0	−2	0	0	0	0	0	0	0	0	0
17	6	6	2	−2	−2	0	0	0	0	0	0	2	2	0	−2	0	0	0	0	0
18	8	−8	0	0	0	−1	1	0	0	0	0	0	0	0	0	1	−1	0	−4	4
19	8	−8	0	0	0	−1	1	0	0	0	0	0	0	0	0	−1	1	0	4	−4

tions Δ^{0p} of $\mathcal{B}(0000)$ are simply those of $\mathcal{B}=S_4$ (or T_d as the group also is called[24]); i.e., there are five different Δ^{0p} matrices with dimensions 1, 1, 2, 3, and 3, respectively. From Eq. (A6) we find that $j,k=1$ and thus we have found five irreducible representations of G_4 with dimensions 1, 1, 2, 3, and 3 of the form $\Gamma^{(0000)p}(ab)=\chi^{(0000)}(a)\Delta^{0p}(b)$.

Next we choose $\mathbf{q}'=(1111)$. We find that, for $\forall a \in \mathcal{A}$, $\forall b \in \mathcal{B}$, $\chi^{(1111)}(bab^{-1})=\Pi_i a^1_{b(i)}=\Pi_j a_j=\chi^{(1111)}(a)$. So in analogy with $\mathbf{q}'=(0000)$ we have $\mathcal{B}(1111)=\mathcal{B}$, and like before we find five irreducible representations of G_4 with dimensions 1, 1, 2, 3, and 3 of the form $\Gamma^{(1111)p}(ab)=\chi^{(1111)}(a)\Delta^{0p}(b)$, with the same Δ^{0p} matrices but different χ prefactors as for $\mathbf{q}'=(0000)$.

We go on with $\mathbf{q}'=(1000)$. This yields $\chi^{(1000)}(bab^{-1})=a_{b(1)}$ which equals $\chi^{(1000)}(a)$ for $\forall a \in \mathcal{A}$ if and only if $b(1)=1$. Thus $\mathcal{B}(1000)$ is the six-element subgroup of $\mathcal{B}$ which leaves the first axis invariant. The coset decomposition of $\mathcal{B}$ contains four terms with coset representatives that each leaves one of the four axis invariant. Not surprisingly we find orb$(1000)=\{(1000),(0100),(0010),(0001)\}$. The little group $\mathcal{B}(1000)$ is isomorphic with C_{3v} and has thus three irreducible representations Δ^{1p} with dimensions 1, 1, and 2, respectively. This combined with the fact that index j,k in Eq. (A6) runs over the four coset representatives means that we have found three more irreducible representations $\Gamma^{(1000)p}$ of G_4 with dimensions 4, 4, and 8, and with entries of the form 0, $\chi^{(1000)}\Delta^{1p}$, $\chi^{(0100)}\Delta^{1p}$, $\chi^{(0010)}\Delta^{1p}$, or $\chi^{(0001)}\Delta^{1p}$.

Then we consider $\mathbf{q}'=(0111)$. The character $\chi^{\mathbf{q}'}$ now gives $\chi^{(0111)}(bab^{-1})=a_{b(2)}a_{b(3)}a_{b(4)}$ which as above equals $\chi^{(0111)}(a)$ for $\forall a \in \mathcal{A}$ if and only if $b(1)=1$. The rest of the analysis is similar as the previous case: orb$(0111)=\{(0111),(1011),(1101),(1110)\}$ and $\mathcal{B}(1000)$ is isomorphic with C_{3v}. We end up with three more irreducible representations $\Gamma^{(0111)p}$ of G_4 with dimensions 4, 4, and 8, having entries of 0, $\chi^{(0111)}\Delta^{1p}$, $\chi^{(1011)}\Delta^{1p}$, $\chi^{(1101)}\Delta^{1p}$, or $\chi^{(1110)}\Delta^{1p}$.

The last choice for $\mathbf{q}'$ turns out to be $\mathbf{q}'=(0011)$, and we obtain $\chi^{(0011)}(bab^{-1})=a_{b(3)}a_{b(4)}$, which equals $\chi^{(0011)}(a)$ for $\forall a \in \mathcal{A}$ if and only if b does not mix the pairs (1,2) with (3,4). It is easily seen that $\mathcal{B}(0011)$ is a four-element group isomorphic with $\mathcal{Z}_2 \otimes \mathcal{Z}_2$, and thus has 4 one-dimensional irreducible representations Δ^{2p}. The coset representation of $\mathcal{B}$ consists of six terms in this case, and orb$(0011)=\{(0011),(0101),(0110),(1001),(1010),(1100)\}$. At this point we note that all 16 possible values of $\mathbf{q}'$ now are a member of an orbit. The six coset representatives combined with the 4 one-dimensional irreducible representations of $\mathcal{B}(0011)$ yield through Eq. (A6) four new irreducible representations of G_4 each being six dimensional and each having entries of the form 0, $\chi^{(1100)}\Delta^{2p}$, $\chi^{(1010)}\Delta^{2p}$, $\chi^{(1001)}\Delta^{2p}$, $\chi^{(0110)}\Delta^{2p}$, $\chi^{(0101)}\Delta^{2p}$, or $\chi^{(0011)}\Delta^{2p}$. In conclusion we see that G_4 has 20 irreducible representations with the dimensions listed in the first column of the character table shown in Table IV. This result is to be contrasted with the list of representation dimensions given in Ref. 20, where only translations and reflections are taken into account in the analysis of the space group of the 4×4 lattice. Note especially the three- and six-dimensional representations found here as opposed to dimensions equal powers of 2 in Ref. 20.

APPENDIX B: THE IRREDUCIBLE REPRESENTATIONS OF G_3, G_5, AND G_6

The irreducible representations R of the space groups G_L with $L=3,5,6$ can be derived analytically following Ref.

TABLE V. The irreducible representations R of G_L for $L=3$, 5, and 6, their corresponding quantum numbers (k_x,k_y,b_x,b_y,c), and their dimensions l_R. The symbol * refers to indefinite reflection quantum numbers.

3×3 lattice

R	0	1	2	3	4	5	6	7	8
k_x	0	0	0	0	0	$\frac{2\pi}{3}$	$\frac{2\pi}{3}$	$\frac{2\pi}{3}$	$\frac{2\pi}{3}$
k_y	0	0	0	0	0	0	0	$\frac{2\pi}{3}$	$\frac{2\pi}{3}$
b_x	1	−1	1	−1	1	*	*	*	*
b_y	1	−1	1	−1	−1	1	−1	*	*
c	1	1	−1	−1	*	*	*	1	−1
l_R	1	1	1	1	2	4	4	4	4

5×5 lattice

R	0	1	2	3	4	5	6	7	8	9	10	11	12	13
k_x	0	0	0	0	0	$\frac{2\pi}{5}$	$\frac{2\pi}{5}$	$\frac{4\pi}{5}$	$\frac{4\pi}{5}$	$\frac{2\pi}{5}$	$\frac{2\pi}{5}$	$\frac{4\pi}{5}$	$\frac{4\pi}{5}$	$\frac{2\pi}{5}$
k_y	0	0	0	0	0	0	0	0	0	$\frac{2\pi}{5}$	$\frac{2\pi}{5}$	$\frac{4\pi}{5}$	$\frac{4\pi}{5}$	$\frac{4\pi}{5}$
b_x	1	−1	1	−1	1	*	*	*	*	*	*	*	*	*
b_y	1	−1	1	−1	−1	1	−1	1	−1	*	*	*	*	*
c	1	1	−1	−1	*	*	*	*	*	1	−1	1	−1	*
l_R	1	1	1	1	2	4	4	4	4	4	4	4	4	8

6×6 lattice

R	0	1	2	3	4	5	6	7	8	9	10	11	12	13	14	15	16	17	18	19	20	21	22	23	24	25	26
k_x	0	π	0	π	0	π	0	π	π	0	π	π	π	π	$\frac{2\pi}{3}$	$\frac{2\pi}{3}$	$\frac{\pi}{3}$	$\frac{\pi}{3}$	$\frac{\pi}{3}$	$\frac{\pi}{3}$	$\frac{2\pi}{3}$	$\frac{2\pi}{3}$	$\frac{2\pi}{3}$	$\frac{2\pi}{3}$	$\frac{\pi}{3}$	$\frac{\pi}{3}$	$\frac{\pi}{3}$
k_y	0	π	0	π	0	π	0	π	0	0	0	π	0	0	0	0	π	π	0	0	π	π	$\frac{2\pi}{3}$	$\frac{2\pi}{3}$	$\frac{\pi}{3}$	$\frac{\pi}{3}$	$\frac{2\pi}{3}$
b_x	1	−1	−1	1	1	−1	−1	1	−1	1	1	1	−1	1	*	*	*	*	*	*	*	*	*	*	*	*	*
b_y	1	−1	−1	1	1	−1	−1	1	1	−1	1	−1	−1	−1	1	−1	−1	1	1	−1	−1	1	*	*	*	*	*
c	1	1	1	1	−1	−1	−1	−1	*	*	*	*	*	*	*	*	*	*	*	*	*	*	1	−1	1	−1	*
l_R	1	1	1	1	1	1	1	1	2	2	2	2	2	2	4	4	4	4	4	4	4	4	4	4	4	4	8

20. In Table V each of them is specified by the lattice size L and by its representation quantum numbers (k_x,k_y,b_x,b_y,c) related to the translation and reflection operators $\{t_x,t_y,r_x,r_y,r_d\}$, respectively. Furthermore, the dimensions l_R of the representations are listed.

APPENDIX C: PROJECTION OPERATORS OF CONTINUOUS SYMMETRIES

There exist several methods for calculating the projection operators corresponding to a continuous symmetry given by a Hermitian operator $\hat{O}$; here we think of $\hat{O}$ as being either the spin operator $\hat{S}^2$ or the pseudospin operator $\hat{J}^2$. In this appendix we present an algorithm based on successive applications of $\hat{O}$. Let $|\phi_0\rangle$ be a given normalized state we want to project into $\hat{O}$-symmetry-invariant subspaces. When $\hat{O}$ acts on $|\phi_0\rangle$ a term proportional with $|\phi_0\rangle$ is generated together with a rest term. The rest term is denoted $f_1|\phi_1\rangle$, and it defines a new unit vector $|\phi_1\rangle$ perpendicular to $|\phi_0\rangle$ while f_1 is a prefactor:

$$\hat{O}|\phi_0\rangle=\langle\phi_0|\hat{O}|\phi_0\rangle|\phi_0\rangle+f_1|\phi_1\rangle. \tag{C1}$$

If $f_1=0$, we are done; if not, we continue by applying $\hat{O}$ to $|\phi_1\rangle$ and expand the result on $|\phi_0\rangle$, $|\phi_1\rangle$. The rest term is now denoted $f_2|\phi_2\rangle$, where $|\phi_2\rangle$ is a unit vector perpendicular to both $|\phi_0\rangle$ and $|\phi_2\rangle$ and f_2 is a prefactor:

$$\hat{O}|\phi_1\rangle=\langle\phi_0|\hat{O}|\phi_1\rangle|\phi_0\rangle+\langle\phi_1|\hat{O}|\phi_1\rangle|\phi_1\rangle+f_2|\phi_2\rangle. \tag{C2}$$

Since we are working in a finite Hilbert space, this process is guaranteed to yield a zero rest term after M steps, i.e., $f_M=0$. The set $S_{\hat{O}}(|\phi_0\rangle)=\{|\phi_0\rangle,|\phi_1\rangle,\ldots,|\phi_{M-1}\rangle\}$ thus yields the smallest $\hat{O}$-invariant subspace containing the starting vector $|\phi_0\rangle$. The symmetry operator $\hat{O}$ is then diagonalized within $S_{\hat{O}}(|\phi_0\rangle)$, yielding the eigenvalues ω_k and eigenvectors $|\omega_k\rangle$:

$$\hat{O}|\omega_k\rangle=\omega_k|\omega_k\rangle, \quad \text{with } |\omega_k\rangle=\sum_{i=0}^{M-1} c_{ki}|\phi_i\rangle. \tag{C3}$$

The projection $\mathcal{P}_{\hat{O}}^{\omega_k}$ of $|\phi_0\rangle$ into the $\hat{O}$-symmetry-invariant subspace corresponding to the eigenvalue ω_k is thus simply

$$\mathcal{P}_{\hat{O}}^{\omega_k}|\phi_0\rangle = c_{k0}^*|\omega_k\rangle. \tag{C4}$$

Based on this equation we find the expressions for the projections in spin space, Eqs. (11)–(13), and in pseudospin space, Eqs. (16)–(21).

APPENDIX D: SIMULTANEOUS EIGENSTATES OF $\hat{T}$ AND $\hat{U}$

In this appendix we present the analytical construction of simultaneous eigenstates of $\hat{T}$ and $\hat{U}$. The existence of these states explains the remaining degeneracies in the symmetry-invariant subspaces, and they (found numerically) are listed in Table III grouped after the $\hat{U}$ eigenvalue γ (=0,1,2 for four-electron systems) and the spin S. We denote these states $\hat{T}/\hat{U}$ states or $|\psi_S^\gamma\rangle$. *A priori*, eigenstates of $\hat{U}$ are most conveniently described in real space whereas eigenstates of $\hat{T}$ are naturally given in momentum space. To require a state to be a $\hat{T}/\hat{U}$ state imposes severe constraints. Below we find many of these states analytically. Since in the following we will be using both real space states and momentum space states, we will reserve the letters a, b, c, and d for sites in real space and the letters k, q, p, and r for momenta.

We begin from below in Table III by studying two-pair states, i.e., $\gamma=2$. In a naive sense, such a state must be a superposition of extremely localized states in real space or correspondingly of very out-spread states in momentum space. This involves superpositions of many states with different wave vectors $\mathbf{k}$ and hence different energies given by Eq. (26). It turns out that to obtain an energy eigenstate state only states where $\mathbf{k}$ enters together with $\boldsymbol{\pi}-\mathbf{k}$, where $\boldsymbol{\pi}=(\pi,\pi)$, can be used since $\cos(k^\zeta)+\cos(\pi-k^\zeta)=0$, and consequently these states only exist for even L. We construct the desired state $|\psi_{S=0}^{\gamma=2}\rangle$ by superposing two-pair states:

$$|\psi_{S=0}^{\gamma=2}\rangle \equiv \sum_{ab} e^{i\boldsymbol{\pi}\cdot(\mathbf{a}+\mathbf{b})}|a,b;a,b\rangle = \sum_{\mathbf{kp}} |\mathbf{k},\mathbf{p};\boldsymbol{\pi}-\mathbf{k},\boldsymbol{\pi}-\mathbf{p}\rangle. \tag{D1}$$

From the real space representation it is seen immediately that $\hat{U}|\psi_{S=0}^{\gamma=2}\rangle = 2|\psi_{S=0}^{\gamma=2}\rangle$ and that $\hat{\mathcal{P}}_S^{(0)}|\psi_{S=0}^{\gamma=2}\rangle = |\psi_{S=0}^{\gamma=2}\rangle$, while the momentum space representation directly yields $\hat{T}|\psi_{S=0}^{\gamma=2}\rangle = 0|\psi_{S=0}^{\gamma=2}\rangle$. In fact, as can be seen in the rows $\gamma=2$ of Table III, this is the only $\hat{T}/\hat{U}$ state with $\gamma=2$; e.g., it is easily seen from Eqs. (11)–(13) that no $\gamma=2$ state can have $S=1$ or 2. Note how $|\psi_{S=0}^{\gamma=2}\rangle$ is independent of the coupling strength U, but that its energy is U dependent and of the form $E(U)=E(0)+2U$.

Having explained the $\gamma=2$ rows of Table III we turn to the $\gamma=1$ rows. From Eqs. (11)–(13) we find that there exist no $\gamma=1$ states with $S=2$. To find the $\gamma=1$ states with $S=0,1$ we construct states $|\psi_{\mathbf{kq}}\rangle$ which manifestly contains exactly one pair, such that $\hat{U}|\psi_{\mathbf{kq}}\rangle = |\psi_{\mathbf{kq}}\rangle$:

$$|\psi_{\mathbf{kq}}\rangle = \sum_a e^{i\boldsymbol{\pi}\cdot\mathbf{a}} e^{i[\mathbf{k}\cdot\mathbf{b}+(\mathbf{q}-\mathbf{k})\cdot\mathbf{d}]}(1-\delta_{b,d})|a,b;a,d\rangle$$

$$= \sum_{\mathbf{p}} |\mathbf{p},\mathbf{k};\boldsymbol{\pi}-\mathbf{p},\mathbf{q}-\mathbf{k}\rangle - \frac{1}{L^2}\sum_{\mathbf{pr}} |\mathbf{p},\mathbf{r};\boldsymbol{\pi}-\mathbf{p},\mathbf{q}-\mathbf{r}\rangle. \tag{D2}$$

Note how the double sum in Eq. (D2) involves all $\mathbf{k}$ vectors but that it only depends on $\mathbf{q}$. To obtain $S=1$ we simply form antisymmetric combinations of such states:

$$|\psi_{\mathbf{kq}}^-\rangle = |\psi_{\mathbf{kq}}\rangle - |\psi_{(\mathbf{q}-\mathbf{k})\mathbf{q}}\rangle$$

$$= \sum_{\mathbf{p}} (|\mathbf{p},\mathbf{k};\boldsymbol{\pi}-\mathbf{p},\mathbf{q}-\mathbf{k}\rangle - |\mathbf{p},\mathbf{q}-\mathbf{k};\boldsymbol{\pi}-\mathbf{p},\mathbf{k}\rangle). \tag{D3}$$

First, we note that $|\psi_{\mathbf{kq}}^-\rangle \neq 0$ if and only if $\mathbf{q}\neq 2\mathbf{k}$. Second, since only permutations of the vectors $\mathbf{k}$ and $(\mathbf{q}-\mathbf{k})$ are involved, we find that $\hat{H}|\psi_{\mathbf{kq}}^-\rangle = E|\psi_{\mathbf{kq}}^-\rangle$. And third, $\hat{\mathcal{P}}_S^{(1)}|\psi_{\mathbf{kq}}^-\rangle = -|\psi_{\mathbf{kq}}^-\rangle$. Thus we have found $\binom{L^2}{2}\hat{T}/\hat{U}$ states $|\psi_{S=1}^{\gamma=1}\rangle$. This yields exactly the number of states listed in the $\gamma=1/S=1$ row of Table III:

$$|\psi_{S=1}^{\gamma=1}\rangle = |\psi_{\mathbf{kq}}^-\rangle. \tag{D4}$$

The states $|\psi_{S=0}^{\gamma=1}\rangle$ must be sought among linear combinations of $|\psi_{\mathbf{kq}}^+\rangle$ defined as

$$|\psi_{\mathbf{kq}}^+\rangle = |\psi_{\mathbf{kq}}\rangle + |\psi_{(\mathbf{q}-\mathbf{k})\mathbf{q}}\rangle$$

$$= \sum_{\mathbf{p}} [|\mathbf{p},\mathbf{k};\boldsymbol{\pi}-\mathbf{p},\mathbf{q}-\mathbf{k}\rangle + |\mathbf{p},\mathbf{q}-\mathbf{k};\boldsymbol{\pi}-\mathbf{p},\mathbf{k}\rangle]$$

$$- \frac{2}{L^2}\sum_{\mathbf{pr}} |\mathbf{p},\mathbf{r};\boldsymbol{\pi}-\mathbf{p},\mathbf{q}-\mathbf{r}\rangle. \tag{D5}$$

The problem now, however, is that the double sum does not vanish, hence preventing the state of being an energy eigenstate. Only upon forming differences $|\psi_{\mathbf{kq}}^+\rangle - |\psi_{\mathbf{k'q}}^+\rangle$ with $\mathbf{k}'\neq\mathbf{k}$ can we get rid of it. But the resulting state will only be an energy eigenstate if $\Sigma_\zeta[\cos(k^\zeta)+\cos(q^\zeta-k^\zeta)]$ equals $\Sigma_\zeta[\cos(k'^\zeta)+\cos(q^\zeta-k'^\zeta)]$. This is easily obtained if $\mathbf{k}'=(q^x-k^x,k^y)$, since then we are only permuting the momentum components.

$$|\psi_{S=0}^{\gamma=1}\rangle = |\psi_{\mathbf{kq}}^+\rangle - |\psi_{\mathbf{k'q}}^+\rangle. \tag{D6}$$

By accident there can also exist other values of $\mathbf{k}'$ which fulfill the requirement, and besides combine pairs such as $|\psi_{\mathbf{kq}}^+\rangle - |\psi_{\mathbf{k'q}}^+\rangle$ we can also in some cases combine three states, $2|\psi_{\mathbf{kq}}^+\rangle - (|\psi_{\mathbf{pq}}^+\rangle + |\psi_{\mathbf{p'q}}^+\rangle)$, or four, $(|\psi_{\mathbf{kq}}^+\rangle + |\psi_{\mathbf{k'q}}^+\rangle) - (|\psi_{\mathbf{pq}}^+\rangle + |\psi_{\mathbf{p'q}}^+\rangle)$, or even more. By a straightforward combinatorial search we find the number of states listed in the $\gamma=1/S=0$ row of Table III, and we have thus identified all states in the $\gamma=1$ rows, and found them to be independent of U but with an energy dependence of the form $E(U)=E(0)+U$.

Finally, we turn to the $\gamma=0$ rows of Table III. First we note that all $S=2$ states of the systems are found here. This is easily proved by noting that the states with

$(S,S_z)=(2,0)$ are formed by applying the spin-lowering operator S_- (which commutes with H) twice to states with $(S,S_z)=(2,2)$. But the latter states cannot contain any doubly occupied sites since that would yield a lower than maximal value of S_z. Clearly, these states as well as their energies are independent of U. Then we consider a large class of energy eigenstates with $S=0,1$ and $\gamma=0$, which does not require the momentum component π, and which therefore accounts for degeneracies for any value of L. Writing $|(k^x,k^y)\rangle=|k^x\rangle\otimes|k^y\rangle$ we construct $\gamma=0$ states $|\phi\rangle$ obeying $\hat{U}|\phi\rangle=0$ by symmetrizing one component, say, the x component, and letting $\hat{\mathcal{P}}_S^{(2)}$ act on the other:

$$|\phi\rangle=|k_1^x,k_2^x;k_3^x,k_4^x\rangle_s\otimes\hat{\mathcal{P}}_S^{(2)}|k_1^y,k_2^y;k_3^y,k_4^y\rangle,$$

$$|k_1^x,k_2^x;k_3^x,k_4^x\rangle_s\equiv|k_1^x,k_2^x;k_3^x,k_4^x\rangle+|k_1^x,k_2^x;k_4^x,k_3^x\rangle+|k_2^x,k_1^x;k_3^x,k_4^x\rangle+|k_2^x,k_1^x;k_4^x,k_3^x\rangle. \tag{D7}$$

Since only momentum permutations enter, $|\phi\rangle$ is clearly an energy eigenstate. The proper spin states are found by the standard projections:

$$|\psi_{S=S'}^{\gamma=0}\rangle=\hat{\mathcal{P}}_S^{(S')}|\phi\rangle. \tag{D8}$$

Simple combinatorics yields 0, 30, 300, and 1680 $S=0$ states and 0, 90, 1050, and 6300 $S=1$ states for $L=3$, 4, 5, and 6, respectively. In analogy with the $\gamma=1$ case many more $\hat{T}/\hat{U}$ states can be constructed for $L=4$ and 6 and $\gamma=0$ when the momentum vector π is taken into account. We give one example of a class of such states. For a given momentum vector $\mathbf{k}=(k^x,k^y)$ we define for $\delta=x,y,xy$ the functions $\pi_\delta(\mathbf{k})$,

$$\pi_x(\mathbf{k})=(k^x+\pi,k^y),\quad \pi_y(\mathbf{k})=(k^x,k^y+\pi),$$

$$\pi_{xy}(\mathbf{k})=(k^x+\pi,k^y+\pi), \tag{D9}$$

based on which we introduce two operators $\hat{\Pi}_\delta^{\sigma,\sigma}$ and $\hat{\Pi}_\delta^{\overline{\sigma},\sigma}$:

$$\begin{aligned}\hat{\Pi}_\delta^{\sigma,\sigma}|\mathbf{k}_1,\mathbf{k}_2;\mathbf{k}_3,\mathbf{k}_4\rangle&=|\mathbf{k}_1,\mathbf{k}_2;\mathbf{k}_3,\mathbf{k}_4\rangle\\&+|\pi_\delta(\mathbf{k}_1),\pi_\delta(\mathbf{k}_2);\mathbf{k}_3,\mathbf{k}_4\rangle\\&+|\mathbf{k}_1,\mathbf{k}_2;\pi_\delta(\mathbf{k}_3),\pi_\delta(\mathbf{k}_4)\rangle\\&+|\pi_\delta(\mathbf{k}_1),\pi_\delta(\mathbf{k}_2);\pi_\delta(\mathbf{k}_3),\pi_\delta(\mathbf{k}_4)\rangle,\\ \hat{\Pi}_\delta^{\overline{\sigma},\sigma}|\mathbf{k}_1,\mathbf{k}_2;\mathbf{k}_3,\mathbf{k}_4\rangle&=|\pi_\delta(\mathbf{k}_1),\mathbf{k}_2;\pi_\delta(\mathbf{k}_3),\mathbf{k}_4\rangle\\&+|\pi_\delta(\mathbf{k}_1),\mathbf{k}_2;\mathbf{k}_3,\pi_\delta(\mathbf{k}_4)\rangle\\&+|\mathbf{k}_1,\pi_\delta(\mathbf{k}_2);\pi_\delta(\mathbf{k}_3),\mathbf{k}_4\rangle\\&+|\mathbf{k}_1,\pi_\delta(\mathbf{k}_2);\mathbf{k}_3,\pi_\delta(\mathbf{k}_4)\rangle.\end{aligned} \tag{D10}$$

Direct inspection shows $\hat{U}(\hat{\Pi}_\delta^{\sigma,\sigma}-\hat{\Pi}_\delta^{\overline{\sigma},\sigma})|\mathbf{k}_1,\mathbf{k}_2;\mathbf{k}_3,\mathbf{k}_4\rangle=0$, and by enforcing certain constraints on all eight momentum components this state also becomes an energy eigenstate with energy $E=0$, while applying the projector $\hat{\mathcal{P}}_S^{(S')}$ renders the correct spin $S=S'$:

$$|\psi_{S=S'}^{\gamma=0}\rangle=\hat{\mathcal{P}}_S^{(S')}(\hat{\Pi}_\delta^{\sigma,\sigma}-\hat{\Pi}_\delta^{\overline{\sigma},\sigma})|\mathbf{k}_1,\mathbf{k}_2;\mathbf{k}_3,\mathbf{k}_4\rangle,$$

with

$$k_n^x=\pi-k_n^y,\quad n=1,2,3,4. \tag{D11}$$

Finally, we note that for lattices containing the momentum $\pi/2$ as is the case for $L=4$, even more $\hat{T}/\hat{U}$ states can be constructed, in accordance with Table III. An example of this can be obtained from Eq. (D11). If, for example, we let $\delta=x$, then it suffices to enforce the constraint $k_n^x=\pm\pi/2$ while allowing any value for the y components. The result is energy eigenstates with energy $E=\Sigma_n\cos(k_n^y)$.

We conclude that many of the $\hat{T}/\hat{U}$ states $|\psi_S^\gamma\rangle$ found numerically have been constructed analytically, and in agreement with the numerical findings all these states are independent of U, while their energies are of the form $E(U)=E(0)+\gamma U$. The analytic constructions reveal that these states are due to a restricted permutation symmetry for the momentum components of states in momentum space.

*Present address: Niels Bohr Institute, Blegdamsvej 17, DK-2100 Copenhagen, Denmark. Electronic aaddress: bruus@nbl.dk

†Electronic address: dauriac@crtbt.polycnrs-gre.fr

[1] E. Dagatto, Rev. Mod. Phys. **66**, 763 (1994).

[2] E. H. Lieb, in *Proceedings of the XIth International Congress of Mathematical Physics*, Paris, 1994, edited by D. Iagolnitzer (International Press, Paris, 1995), pp. 392–412.

[3] P. W. Anderson, Science **235**, 1196 (1987).

[4] M. Fabrizio, A. Parola, and E. Tosatti, Phys. Rev. B **44**, 1033 (1991).

[5] M. Faas, B. D. Simons, X. Zotos, and B. L. Altshuler, Phys. Rev. B **48**, 5439 (1993).

[6] M. L. Mehta, *Random Matrices*, 2nd ed. (Academic Press, San Diego, 1991).

[7] F. Haake, *Quantum Signatures of Chaos* (Springer-Verlag, Berlin, 1991).

[8] Y. Imry, Europhys. Lett. **1**, 249 (1986); A. D. Stone, P. A. Mello, K. A. Muttalib, and J.-L. Pichard, in *Mesoscopic Phenomena in Solids*, edited by B. L. Altshuler, P. A. Lee, and R. A. Webb (North-Holland, Amsterdam, 1991), Chap. 9.

[9] A. Kudrolli, V. Kidambi, and S. Sridhar, Phys. Rev. Lett. **75**, 822 (1995).

[10] C. Ellegaard *et al.*, Phys. Rev. Lett. **77**, 4918 (1996).

[11] M. V. Berry, Nonlinearity **1**, 399 (1988).

[12] R. Blümel and U. Smilansky, Phys. Rev. Lett. **60**, 477 (1988).

[13] H. Meyer, J.-C. Anglès d'Auriac, and H. Bruus, J. Phys. A **29**, L483 (1996).

[14] R. Mélin, J. Phys. (France) I **6**, 469 (1996).

[15] G. Montambaux, D. Poilblanc, J. Bellisard, and C. Sire, Phys. Rev. Lett. **70**, 497 (1993).

[16] R. Berkovits and Y. Avishai, J. Phys. Condens. Matter **8**, 389 (1996).

[17] T. Hsu and J.-C. Anglès d'Auriac, Phys. Rev. B **47**, 14 291 (1993).

[18] R. Mélin, B. Douçot, and P. Butaud, J. Phys. (France) I **4**, 737 (1994).

[19] H. Bruus and J.-C. Anglès d'Auriac, Europhys. Lett. **35**, 321 (1996).

[20] G. Fano, F. Ortolani, and A. Parola, Phys. Rev. B **46**, 1048 (1992).

[21] A. Pandey, Ann. Phys. (N.Y.) **119**, 170 (1979).

[22] H. Meyer, J.-C. Angès d'Auriac, and J.-M. Maillard, Phys. Rev. E (to be published).

[23] M. Tinkham, *Group Theory and Quantum Mechanics* (McGraw-Hill, New York, 1964).

[24] J. F. Cornwell, *Group Theory in Physics*, (Academic Press, London, 1989), Vols. 1–3.

[25] Y. Hasagawa and D. Poilblanc, Phys. Rev. B **40**, 9035 (1989).

[26] A group G is a direct product group if it possesses two subgroups G_1 and G_2 such that (i) $\forall g \in G \ \exists g_1 \in G_1 \ \exists g_2 \in G_2 : g = g_1 g_2$, (ii) $G_1 \cap G_2 = e$ (e is the identity), (iii) $\forall g_1 \in G_1 \ \forall g_2 \in G_2 : g_1 g_2 = g_2 g_1$. One then writes $G = G_1 \otimes G_2$.

[27] A group G is a semidirect product group if it possesses two subgroups G_1 and G_2 such that (i) $\forall g \in G \ \exists g_1 \in G_1 \ \exists g_2 \in G_2 : g = g_1 g_2$, (ii) $G_1 \cap G_2 = e$, (iii) G_1 is an invariant subgroup, i.e., $\forall g_1 \in G_1 \ \forall g \in G : g g_1 g^{-1} \in G_1$. One then writes $G = G_1 \circledS G_2$.

[28] Using standard cycle notation an example of two permutations generating all of G_4 is (4,12)(5,13)(6,14)(7,15) and (0,4,8,9,10,14,2,3)(1,7,12,5,11,13,6,15).

[29] O. J. Heilmann and E. H. Lieb, Trans. NY Acad. Sci. **33**, 116 (1970).

[30] C. N. Yang, Phys. Rev. Lett. **63**, 2144 (1989).

[31] C. N. Yang and S. C. Zhang, Mod. Phys. Lett. B **4**, 759 (1990).

[32] The symmetrized Hubbard model $\hat{H}'$ is obtained by the substitution $\hat{U} \rightarrow \hat{U}' = \Sigma_i (\hat{n}_{i\uparrow} - \frac{1}{2})(\hat{n}_{i\downarrow} - \frac{1}{2})$, leading to $\hat{H}' = \hat{H} + u(L^2/4 - \Sigma_{i\sigma} \hat{n}_{i\sigma}/2)$.

[33] The pseudospin symmetry can be viewed as a consequence of a particle-hole symmetry which maps a Hubbard model H with coupling strength U and n_u (n_d) spin-up (spin-down) electrons onto a Hubbard model $\widetilde{H}$ with $\widetilde{U} = -U$, $\widetilde{n}_u = n_u$, and $\widetilde{n}_d = L^2 - n_d$. The pseudospin of H is the spin of $\widetilde{H}$ and vice versa (Ref. 2).

[34] B. L. Al'tshuler and B. I. Shklovskiĭ, Zh. Eksp. Teor. Fiz. **91**, 220 (1986) [Sov. Phys. JETP **64**, 127 (1986)].

[35] M. V. Berry, Proc. R. Soc. **400**, 229 (1991).

[36] D. Weinmann and J.-L. Pichard, Phys. Rev. Lett. **77**, 1556 (1996).